Generalized run-and-turn motions: From bacteria to Lévy walks

François Detcheverry
Univ Lyon, Université Claude Bernard Lyon 1, CNRS, Institut Lumière Matière, F-69622 Villeurbanne, France
(Received 26 January 2017; published 26 July 2017)

Swimming bacteria exhibit a repertoire of motility patterns, in which persistent motion is interrupted by turning events. What are the statistical properties of such random walks? If some particular instances have long been studied, the general case where turning times do not follow a Poisson process has remained unsolved. We present a generic extension of the continuous time random walks formalism relying on operators and noncommutative calculus. The approach is first applied to a unimodal model of bacterial motion. We examine the existence of a minimum in velocity correlation function and discuss the maximum of diffusivity at an optimal value of rotational diffusion. The model is then extended to bimodal patterns and includes as particular cases all swimming strategies: run-and-tumble, run-stop, run-reverse and run-reverse-flick. We characterize their velocity correlation functions and investigate how bimodality affects diffusivity. Finally, the wider applicability of the method is illustrated by considering curved trajectories and Lévy walks. Our results are relevant for intermittent motion of living beings, be they swimming micro-organisms or crawling cells.

DOI: 10.1103/PhysRevE.96.012415

I. INTRODUCTION

Many bacteria are relentless microswimmers [1–4]. Their trajectories often involve persistent swimming punctuated by sudden reorientation events. A variety of distinct movement patterns have now been identified [5–8]. In this work, we answer what may be the simplest question about those random motions [9]. What are their statistical properties? For instance, how can we compute the mean square displacement and diffusivity?

The swimming ability of many bacteria rests on a common apparatus: one or several flagella, each powered by a rotary motor embedded in the membrane [10,11]. Unlike its eukaryotic pendant, whose internal motors generate active deformation, the bacterial flagellum is a passive filament. It is also a polymorphic structure which can adopt a discrete set of helical shapes [12]. Several configurations are possible for the arrangement of flagella: monotrichous bacteria, which include the majority of marine species [13], possess a single polar flagellum, whereas peritrichous bacteria have multiple flagella placed at random positions over the body. If in some mutant strains motors are unceasingly in action and trajectories are smooth, many bacterial motors operate discontinuously, resulting in intermittent patterns of motion.

The most studied swimming strategy is probably the run-and-tumble of *Escherichia coli*, a peritrichous bacterium that inhabits the large intestine of humans and other warm-blooded animals [1,5]. When all motors rotate counterclockwise, flagella bundle into a helical filament. During this "run," the cell is propelled forward in near straight motion with a velocity in the range 10–30 $\mu m\, s^{-1}$. If one or several motors switch to clockwise rotation, the flagella unbundle, inducing a rapid change of direction. Such "tumble" is not isotropic, with an average turning angle of 70°.

Swimming patterns are not restricted to run-and-tumble, but rather a theme with variations. The simplest instance may be the run-stop of *Rhodobacter sphaeroides*, whose single unidirectional motor periodically pauses. At each motor stop, the flagellum switches from a helical to a coiled state, inducing active reorientation of the cell [6,14]. Prevalent among marine bacteria such as *Pseudoalteromonas haloplanktis* [15], the run-reverse pattern is based on a bidirectional motor, that recurrently changes its direction of rotation, alternating between pushing and pulling modes. The soil bacterium *Pseudomonas putida* adds its own variation, with swimming velocities in the forward and reverse directions that differ by an average factor of 2 [8]. Finally, some monotrichous bacteria employ the run-reverse-flick pattern recently uncovered in the marine bacterium *Vibrio alginolyticus*, and which involves a three-step cycle: run forward, then backward, and flick [7]. The latter is a sudden reorientation that is triggered by a mechanical instability of the hook [16], with an average turning angle close to 90°. To encompass all types of swimming strategies in a single term, it may be convenient to call them run-and-turn motions [17].

The knowledge of swimming patterns has benefited from recent advances in experimental techniques, including microfluidics [2]. Alongside high-throughput approaches to characterize population motility such as differential dynamic microscopy [18], sophisticated methods are developed for three-dimensional (3D) tracking of individual bacteria, relying on holography or diffraction pattern analysis [19,20]. Together with progress on trajectory analysis [21], they give access to unprecedented characterization of trajectories, with full statistics on properties such as turning angle or run time distributions.

Quantitative observations of bacterial run-and-turn motions raise a myriad of questions. A first line of research investigates the mechanisms at play in propulsion. A full understanding involves uncovering a multiplicity of aspects: from the hydrodynamics of swimming [3,4] to the mechanics of flagellum or hook and polymorphic transitions [12,16], but also the motor machinery or biochemical regulation [6,22,23] and the swimming efficiency and optimality [4,24]. Equally important is a second line of research, concerned with the properties of motility patterns, which underlie essential microbial actions such as chemotactic ability, pathogenicity, and foraging efficiency. Given that bacteria appeared three billion years ago, it is a natural hypothesis that evolution may have shaped

patterns for a specific environment. Which benefits then come with a particular pattern? Before such a broad question can be answered, a prerequisite is to characterize the basic properties of bacteria random motions. This is the issue we address here.

The literature on random walks is vast, to say the least. Not only a cornerstone of statistical physics, it has developed ramifications in various fields, including mathematics, biology, and ecology [9,25–27] and continues to explore countless variations. Let us point out some distinguishing features of run-and-turn motions. First, contrary to self-avoiding or reinforced random walks [28,29] they are noninteracting. Second, they occur in continuous space and time. The latter is in contrast with random walks defined by discrete steps as in the original Pearson problem [30–32]. Finally, they include discontinuous changes, the turning events, which are approximated as instantaneous, and retain memory, since directions before and after the turn are, in general, correlated.

Run-and-turn patterns may be divided in two classes: Poissonian or non-Poissonian. In the former, turning events follow a Poisson process, with a rate constant in time and a distribution of run time which is exponential. The Poissonian case has been fully explored, for multiple reasons. In the context of bacteria, the run-and-tumble of *E. coli*, which has become one model organism for motility and chemotactic properties [1], proved to be Poissonian in the early observations [5], as also found in more recent studies [20,33]. On the theoretical side, the Poissonian process, being maximally random [34], may appear as the simplest assumption. It also arises naturally in physical models of particle propagation, such as the Lorentz model of electrons where ballistic motion is interspersed with collision events that randomize the direction [35]. Last but not least, Poissonian run-and-turn motions are in general more tractable, since they involve equations that are local in time, with no memory kernel. Accordingly, the Poissonian class has been thoroughly investigated in various situations [36–39], including swimming patterns [40,41].

There has been growing evidence that the non-Poissonian class, while rather neglected in the past, is fully relevant to swimming bacteria. Instead of a monotonic decay, the run time distribution can exhibit a peak, as reported in a number of species, including *E. coli* [42], *V. alginolyticus* [7,43], *P. putida* [8,44], and *Caulobacter crescentus* [45]. The presence of a maximum generically suggests that motor switching is an out of equilibrium process [46]. Microscopic models for dynamic binding of proteins to motor subunits may also predict nonexponential run time, governed for instance by first passage statistics [45]. Even for a Poissonian switching of the motor, the polymorphic transitions of flagella and the influence of mechanical load on switching rate may lead to a peak in run time [47]. Finally, though exponential tails are frequently observed for the run time distribution [7,43,45], power laws have also been reported [48], and rationalized theoretically by the interplay between noise and nonlinearity in signaling pathway [23,49].

In comparison to its Poissonian counterpart, the class of non-Poissonian run-and-turn has proven more challenging to address theoretically. Because of memory in the process, a Fokker-Planck approach yields an intricate integrodifferential equation [50,51]. A framework that from the outset could treat arbitrary time distribution is the continuous time random walks (CTRWs), introduced in 1965 by Montroll and Weiss [52,53]. Initially developed for on-lattice random walks involving a series of jumps separated by waiting periods, the formalism was later extended to tackle continuous random motions occurring during a run, but only under the restriction that each turning event implies a complete decorrelation in the direction of motion [39,54,55]. This assumption is invalid for most, if not all, swimming patterns. As a result, and in spite of some progress [41,56], non-Poissonian run-and-turn patterns have eluded comprehensive treatment.

In this study, we propose a generic framework to address run-and-turn motions, Poissonian or not, as found in bacterial swimming patterns. We present in Sec. II a formalism that extends the CTRWs to operators and introduce the necessary tools of noncommutative calculus. In Sec. III, we apply the method to a simple, unimodal model of run-and-turn and explain how to obtain the statistical properties of motion for arbitrary distribution of run time. We discuss the minimum that may exist in velocity correlation function and the maximum of diffusivity arising at a finite value of rotational diffusion coefficient. The extension to bimodal run-and-turn, which is required to describe all types of swimming patterns, is given in Sec. IV. We examine to which extent patterns differ in their velocity correlation functions and show that diffusivity is expected to be reduced by bimodality in angle but enhanced by bimodality in velocity. Finally, Sec. V is a direct application of our technique to intrinsically curved trajectories and to Lévy walks, for which features of the one-dimensional case are shown to hold in dimensions 2 and 3. Section VI provides a summary and points out the relevance to other motility patterns, from individual cells to higher organisms.

A preliminary account of this work appeared in Ref. [57]. Here we expand on this earlier study in several respects. We present a self-contained description of the formalism and explain in detail the steps involved in the method, including the noncommutative differentiation. We also consider numerous instances of applications of the run-and-turn model, from bacterial patterns to Lévy walks. Finally, we provide a full discussion of the results, focusing in particular on the maximization of diffusivity.

II. FORMALISM

This section presents a generic framework that is an extension of CTRWs. While the derivation closely parallels the traditional formalism, the difference lies in the introduction of operators which may be noncommutative. The approach is not restricted to the study of random motions but may prove useful in the numerous domains where CTRWs have already found applications, including solid-state physics, protein folding, earthquakes and hydrology, or financial markets [58–60].

A. Extending the CTRWs to operators

We consider a system whose state, specified by a vector $\mathbf{x}$, changes in time in two distinct ways. On the one hand, the "run" is a continuous evolution during which the probability density $p(\mathbf{x},t)$ is governed by the Liouvillian $\mathcal{L}$ according to $\partial_t p = \mathcal{L} p$ [61]. On the other hand, the "jump" is an instantaneous change of state defined by convolution with

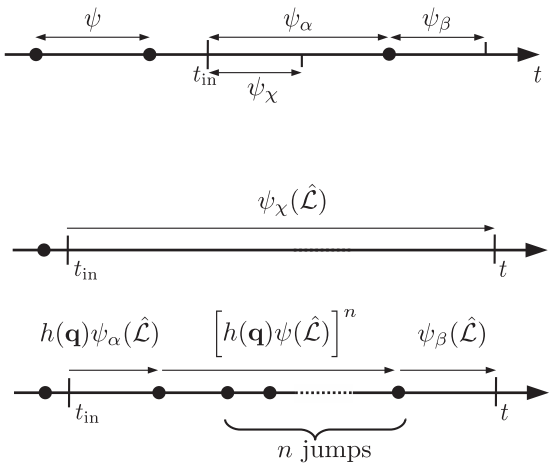

FIG. 1. Top: Schematics for the run time distribution ψ and the derived quantities ψ_α, ψ_β, and ψ_χ defined in the text and given by Eq. (1). $t_{\rm in}$ is the randomly chosen initial time, each dot indicates a jump event. Bottom: Graphical interpretation of the two terms appearing in $P(\mathbf{q},s)$ as given by Eq. (7).

a kernel $h(\mathbf{x})$. As a simple example, the state $\mathbf{x}$ could be the position of a moving particle, the run could involve pure diffusive motion, in which case the Liouvillian is the Laplacian ∇^2 and the jump could describe instantaneous hops, with a distribution $h(\mathbf{x})$ of displacements.

The jump events are governed by a renewal process: the intervals between two successive jumps are independently drawn from a run time distribution $\psi(t)$. We assume that the process began at a time infinitely remote in the past and that the mean run time is finite, so that a steady state is reached. The initial time of observation $t_{\rm in}$ is then chosen at random [55,62,63]. This steady state assumption requires the introduction of several additional quantities [64]: the probability density $\psi_\alpha(t)$ for the forward waiting (or recurrence) time, meaning that the next jump comes about a time t after $t_{\rm in}$, the probability $\psi_\beta(t)$ that the run time exceeds t, and the probability $\psi_\chi(t)$ that no jump occurs for a time t after $t_{\rm in}$. Those quantities, which are illustrated in Fig. 1, can be expressed as [39]

$$\begin{aligned}
\psi_\alpha(t) &= \frac{\psi_\beta(t)}{\tau}, & \psi_\alpha(s) &= \frac{\psi_\beta(s)}{\tau},\\
\psi_\beta(t) &= \int_t^\infty dt'\psi(t'), & \psi_\beta(s) &= \frac{1-\psi(s)}{s}, \qquad (1)\\
\psi_\chi(t) &= \int_t^\infty dt'\frac{t'-t}{\tau}\psi(t'), & \psi_\chi(s) &= \frac{\psi(s)+\tau s-1}{\tau s^2}.
\end{aligned}$$

Here, τ is the mean run time and s is the variable for the Laplace transform with respect to time, as defined in Appendix A.

Given a probability density of initial state $P_{\rm in}(\mathbf{x})$, the goal is to find the probability density $P(\mathbf{x},t)$ at a later time t. To do so, let us introduce the run propagator characterizing the continuous evolution, $p(\mathbf{x},\mathbf{x}',t-t')$, that is the probability density to be in state $\mathbf{x}$ at time t given state $\mathbf{x}'$ at time t', assumed time invariant. We also need the joint probability density $J(\mathbf{x},t)$ that the system jumps to state $\mathbf{x}$ precisely at time t. Choosing from now on $t_{\rm in}=0$, $P(\mathbf{x},t)$ and $J(\mathbf{x},t)$ satisfy

$$J(\mathbf{x},t)=\int_0^t dt'\psi(t-t')\int d\mathbf{x}'h(\mathbf{x}-\mathbf{x}')\int d\mathbf{x}''p(\mathbf{x}',\mathbf{x}'',t-t')J(\mathbf{x}'',t')+\psi_\alpha(t)\int d\mathbf{x}'h(\mathbf{x}-\mathbf{x}')\int d\mathbf{x}''p(\mathbf{x}',\mathbf{x}'',t)P_{\rm in}(\mathbf{x}''), \quad (2)$$

$$P(\mathbf{x},t)=\int_0^t dt'\psi_\beta(t-t')\int d\mathbf{x}'p(\mathbf{x},\mathbf{x}',t-t')J(\mathbf{x}',t')+\psi_\chi(t)\int d\mathbf{x}'p(\mathbf{x},\mathbf{x}',t)P_{\rm in}(\mathbf{x}'). \quad (3)$$

The first contribution to $J(\mathbf{x},t)$ collects all trajectories that included a jump to state $\mathbf{x}''$ at time t', then evolved continuously up to time t to reach state $\mathbf{x}'$, at which point they jumped to state $\mathbf{x}$. The run time in this case is $t-t'$, whence the $\psi(t-t')$ factor. Because $\mathbf{x}'$, $\mathbf{x}''$, and t' may be chosen arbitrarily, triple integration is performed over those variables. The second contribution to $J(\mathbf{x},t)$ corresponds to trajectories where not a single jump took place before t, resulting in the $\psi_\alpha(t)$ factor. Continuous evolution brought the system from the initial state $\mathbf{x}''$ to $\mathbf{x}'$, before a jump to $\mathbf{x}$ occurs precisely at time t. As regards $P(\mathbf{x},t)$, the first and second terms arise in an identical manner, accounting respectively for the cases where in the time interval $[0,t[$ there is at least one jump event or none.

Moving to transformed variables allows us to convert those equations into a tractable form. Laplace transforms are used for the time variable ($t\to s$), so that convolution translates into a product. With the appropriate transform ($\mathbf{x}\to\mathbf{q}$), which depends on the particular system under study, convolutions in the $\mathbf{x}$ variable are also turned into multiplication. Those two steps are standard in CTRWs. The third and unusual step is to introduce the operator representation for the run propagator $p(\mathbf{x},\mathbf{x}',t-t')$ [50]:

$$e^{(t-t')\mathcal{L}}f(\mathbf{x},t')=\int d\mathbf{x}'p(\mathbf{x},\mathbf{x}',t-t')f(\mathbf{x}',t'), \quad (4)$$

indicating that upon action of the operator $e^{(t-t')\mathcal{L}}$, the probability density $f(\mathbf{x},t')$ evolves for a time span $t-t'$, thus reaching time t. With this representation, integrals of the type $\int_0^t dt'g(t-t')\int d\mathbf{x}'p(\mathbf{x},\mathbf{x}',t-t')f(\mathbf{x}',t')$ are reduced to the concise expression $g(s-\mathcal{L})f(\mathbf{x},s)$. Details for this calculation can be found in Appendix B 1. Once all three steps are performed, the lengthy Eqs. (2) and (3) take the compact form

$$J(\mathbf{q},s)=h(\mathbf{q})\psi(\hat{\mathcal{L}})J(\mathbf{q},s)+h(\mathbf{q})\psi_\alpha(\hat{\mathcal{L}})P_{\rm in}(\mathbf{q}), \quad (5)$$

$$P(\mathbf{q},s)=\psi_\beta(\hat{\mathcal{L}})J(\mathbf{q},s)+\psi_\chi(\hat{\mathcal{L}})P_{\rm in}(\mathbf{q}), \quad (6)$$

with the shorthand notation $\hat{\mathcal{L}}=s-\mathcal{L}$. At this point, reverting to time variable would produce an integrodifferential equation [50,51,65]. Here we follow a different route and keeping in

mind that operators may not commute, we solve Eqs. (5) and (6) to arrive at the generating function, the main equation of this section,

$$P(\mathbf{q},s) = \left[\psi_\chi(\hat{\mathcal{L}}) + \frac{\overset{3}{\psi_\beta}(\hat{\mathcal{L}})[h(\mathbf{q})\psi_\alpha(\hat{\mathcal{L}})]}{[1 - h(\mathbf{q})\psi(\hat{\mathcal{L}})]} \right] P_{\rm in}(\mathbf{q}). \quad (7)$$

Here the order in which a single or a group of operators are taken is specified with Feynman indices [66]. Only their relative value is relevant, with smaller indices coming first. If not indicated otherwise by indices, operators within brackets are applied starting with the rightmost and ending with the leftmost. Once endowed with indices, operators can be manipulated as ordinary commuting quantities.

Equation (7) gives the required probability density $P(\mathbf{q},s)$ in terms of transformed variables, for arbitrary Liouvillian, jump kernel, and run time distribution. A simple graphic interpretation is shown in Fig. 1. There are two separate contributions to $P(\mathbf{q},s)$. If no jump takes place, the operator $\psi_\chi(\hat{\mathcal{L}})$ is applied on the initial distribution $P_{\rm in}(\mathbf{q})$. If at least one jump occurs, three successive stages may be distinguished: the first operator $h(\mathbf{q})\psi_\alpha(\hat{\mathcal{L}})$ describes the evolution up to the first jump, included. A number n of jumps may happen subsequently, each yielding a factor $h(\mathbf{q})\psi(\hat{\mathcal{L}})$. Accounting for all possible n yields $\sum_{n=0}^{\infty}[h(\mathbf{q})\psi(\hat{\mathcal{L}})]^n = [1 - h(\mathbf{q})\psi(\hat{\mathcal{L}})]^{-1}$. The final stage, which follows the ultimate jump, brings the last operator $\psi_\beta(\hat{\mathcal{L}})$.

Two remarks are in order to conclude this section. First, the particular cases of Eq. (7) are easily checked. In the absence of jumps ($h(\mathbf{q}) = 1$), the continuous evolution $P(\mathbf{q},t) = e^{t\mathcal{L}}P_{\rm in}(\mathbf{q})$ is recovered as expected. In the absence of runs ($\mathcal{L} = 0$), there is only a single operator corresponding to jumps, hence ensuring commutativity and leading to the traditional expression of CTRWs with jumps only. Second, the above expression is valid with the assumption of steady state. If, as in the original Montroll-Weiss equation, the initial time $t_{\rm in}$ is chosen to coincide with a jump event, the resulting generating function is

$$P_{\rm ns}(\mathbf{q},s) = \psi_\beta(\hat{\mathcal{L}})[1 - h(\mathbf{q})\psi(\hat{\mathcal{L}})]^{-1}P_{\rm in}(\mathbf{q}), \quad (8)$$

which derives from Eq. (7) by replacing ψ_χ and ψ_α with ψ_β and ψ respectively. The nonsteady state assumption may lead to ergodicity breaking and ageing effects [67], that will not be considered in this work, except briefly in Sec. V B.

B. Noncommutative calculus

Taking the inverse transforms on $P(\mathbf{q},s)$ would yield the probability density in terms of original variables $(\mathbf{x},t)$. Because this step is generally intractable, one instead focuses on moments. Consider a simple example where the state $\mathbf{x} = (x,y,z)$ is a three-dimensional position and $\mathbf{k}$ is the conjugated variable for Fourier transform (see Appendix A). Since $P(\mathbf{k},s)$ is the generating function of moments, the nth moment of abscissa x is obtained from

$$\langle x^n(s)\rangle = \lim_{\mathbf{k}\to 0}\left(-i\frac{\partial}{\partial k_x}\right)^n P(\mathbf{k},s), \quad (9)$$

where $\langle . \rangle$ indicates an ensemble average. In contrast to the usual framework of CTRWs, Eq. (7) for $P(\mathbf{q},s)$ involves not only functions, but operators, which may not commute with one another nor with their own derivative. As a consequence, the differentiation requires some tools of noncommutative analysis, namely the difference derivative and Daletskii-Krein formula [68].

The difference derivative is defined as

$$\delta f(x,y) = \int_0^1 du\, f'[ux + (1-u)y], \quad (10)$$

which, more explicitly, includes the two cases

$$\delta f(x,y) = \frac{f(x) - f(y)}{x - y} \quad \text{if } x \neq y, \quad (11a)$$

$$= f'(x) \quad \text{if } x = y. \quad (11b)$$

The difference derivative of order n is defined by recurrence $\delta^n f = \delta(\delta^{n-1} f)$ and is invariant with respect to permutation of the arguments. When all arguments are distinct, only differences are involved,

$$\delta^n f(x_1, \ldots, x_{n+1}) = \sum_{i=1}^{n+1} \frac{f(x_i)}{\prod_{\substack{j=1,\\ j\neq i}}^{n+1}(x_i - x_j)}. \quad (12)$$

When all arguments are identical, one recovers the usual derivative up to a factorial

$$\delta^n f(x, \ldots, x) = \frac{f^{(n)}(x)}{n!}. \quad (13)$$

The general case interpolates between those two extremes.

The Daletskii-Krein formula indicates how to differentiate a function of an operator, $f(\mathrm{A})$, when the operator A and its derivative A′ do not commute,

$$\frac{d}{dt}f(\mathrm{A}(t)) = \overset{2}{\mathrm{A}}{}' \, \delta f\big(\overset{1}{\mathrm{A}},\overset{3}{\mathrm{A}}\big) = \overset{2}{\mathrm{A}}{}' \, \frac{\overset{1}{f}(\mathrm{A}) - \overset{3}{f}(\mathrm{A})}{\overset{1}{\mathrm{A}} - \overset{3}{\mathrm{A}}}. \quad (14)$$

Extension to higher derivatives is embodied in the Newton formula: if A and B are operators and ϵ is the expansion parameter,

$$f(\mathrm{A} + \epsilon\mathrm{B}) - f(\mathrm{A}) = \sum_{n=1}^{\infty} \epsilon^n \, \overset{2}{\mathrm{B}}\overset{4}{\mathrm{B}} \ldots \overset{2n}{\mathrm{B}} \, \delta^n f(\overset{1}{\mathrm{A}},\overset{3}{\mathrm{A}}, \ldots, \overset{2n+1}{\mathrm{A}}). \quad (15)$$

While a rigorous approach can be found in Ref. [68], here we present a heuristic derivation of the Daletskii-Krein formula. We consider the first order expansion $f(\mathrm{A} + \epsilon\mathrm{B}) = f(\mathrm{A}) + \epsilon\mathrm{T}_1 + O(\epsilon^2)$, where T_1 is the linear part, and focus on the particular case $f(\mathrm{A}) = \mathrm{A}^n$, for which

$$\mathrm{T}_1 = \lim_{\epsilon\to 0}\frac{d}{d\epsilon}f(\mathrm{A} + \epsilon\mathrm{B}) = \sum_{m=0}^{n-1}\mathrm{A}^m\mathrm{B}\mathrm{A}^{n-1-m}. \quad (16)$$

One can check that $\mathrm{A}\mathrm{T}_1 - \mathrm{T}_1\mathrm{A} = \mathrm{A}^n\mathrm{B} - \mathrm{B}\mathrm{A}^n$. Because operators equipped with indices can be treated as usual scalars, an equivalent expression for this equality is

$$\mathrm{T}_1 = \overset{2}{\mathrm{B}}\,\frac{\overset{1}{(\mathrm{A})^n} - \overset{3}{(\mathrm{A})^n}}{\overset{1}{\mathrm{A}} - \overset{3}{\mathrm{A}}}. \quad (17)$$

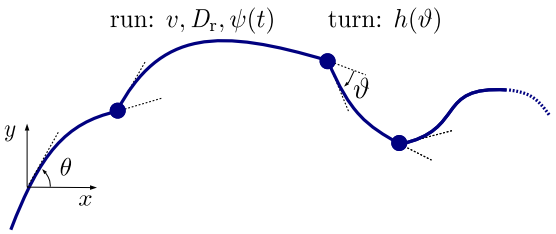

FIG. 2. Unimodal run-and-turn motion in dimension $d = 2$, and its parameters. Runs are characterized by a velocity v, a rotational diffusion coefficient D_r, and a run time distribution $\psi(t)$. Turning events, represented by dots, are specified by the distribution of turning angle $h(\vartheta)$.

By linearity, the above argument immediately extends to functions that can be represented as a power series $f(\mathrm{A}) = \sum_{n=0}^{\infty} a_n \mathrm{A}^n$. Hence, consistent with Eq. (14), one obtains

$$\lim_{\epsilon\to 0} \frac{d}{d\epsilon} f(\mathrm{A}+\epsilon\mathrm{B}) = \overset{2}{\mathrm{B}}\, \frac{\overset{1}{f(\mathrm{A})} - \overset{3}{f(\mathrm{A})}}{\overset{1}{\mathrm{A}} - \overset{3}{\mathrm{A}}}. \tag{18}$$

III. UNIMODAL RUN-AND-TURN

A. Model and method

The generic formalism of Sec. II is now applied to a specific model of bacterial swimming, which is illustrated in Fig. 2 and referred to as unimodal run-and-turn motion. The bacterium, moving in space of dimension $d = 2$ or 3, is characterized by its position and orientation. Runs involve smooth persistent motion, with velocity of constant modulus v, a direction governed by rotational diffusion with coefficient D_r and a run time distribution $\psi(t)$. Jumps are instantaneous reorientations leaving the position unaffected, with a distribution of turning angle h assumed symmetric when $d = 2$ and azimuthally symmetric when $d = 3$ [69].

The model has been investigated previously [40,41] and includes as particular cases the ballistic motion with isotropic turns [55], the run-reverse pattern [70], and some instances of Lévy walks [71]. In the context of bacteria, three assumptions may be discussed. First, the velocity is constant in magnitude. While fluctuations may be seen within a run and from one run to the next [8], taking them into account would represent the next level of refinement. Second, turning events are treated as instantaneous, a reasonable approximation if they are, on average, at least ten times shorter than runs [43]. Because this assumption does not always hold [5], it will be relaxed in Sec. IV with the bimodal model. Finally, run times are independent variables. Such renewal character is supported by the absence of strong correlation between successive run times [43] and by the invariance of properties upon reshuffling run intervals [42]. Note however that correlated run times have also been reported in experimental data and rationalized theoretically [23].

We now explain the method and to do so in the simplest manner, we first focus on the model in dimension $d = 2$. The continuous evolution during a run is governed by the Fokker-Planck equation on $p(\mathbf{r},\theta,t)$,

$$\partial_t p = \mathcal{L}p = D_r\, \Delta_a p - v\, \mathbf{u}\cdot\boldsymbol{\nabla}_{\mathbf{r}} p. \tag{19}$$

Here, θ is the orientation angle and $\mathbf{u} = (\cos\theta, \sin\theta)$ is the orientation vector, $\boldsymbol{\nabla}_{\mathbf{r}}$ is the gradient with respect to position $\mathbf{r} = (x,y)$, and $\Delta_a = \partial^2_{\theta\theta}$ is the angular part of the Laplacian. To proceed, the Liouvillian $\mathcal{L}$ is converted to a tractable form by switching to transformed variables: Fourier transform is taken for position ($\mathbf{r} \to \mathbf{k}$), Fourier series for orientation ($\theta \to l$), and Laplace transform for time ($t \to s$), all of which are defined in Appendix A. In this new basis, the Liouvillian acting on $p(\mathbf{k},l,s)$ does not involve partial derivatives anymore,

$$\mathcal{L} = D_r \Delta_a + \frac{iv}{2}(k_x \mathrm{T}^+ + k_y \mathrm{T}^-), \tag{20}$$

where for an arbitrary function f,

$$\Delta_a f(l) = -l^2 f(l), \quad \mathrm{T}^{\pm} f(l) = \frac{f(l-1) \pm f(l+1)}{i^{(1\mp 1)/2}}, \tag{21}$$

indicating that Δ_a and $\mathrm{T}^{\pm}$ are respectively multiplicative and shifting operators for the l variable. Besides, convolution with the reorientation kernel $h(\mathbf{r},\theta) = \delta(\mathbf{r})h(\theta)$ gives rise to multiplication by $2\pi h(l)$ [72]. The probability density $P(\mathbf{k},l,s)$, as obtained from Eq. (7) with $\mathcal{L}$ from Eq. (20), is the generating function for moments. Hence, for instance,

$$\langle x^n(s)\rangle = 2\pi \lim_{\substack{\mathbf{k}\to\mathbf{0}\\ l\to 0}} \left(-i\frac{\partial}{\partial k_x}\right)^n P(\mathbf{k},l,s). \tag{22}$$

Because the operators Δ_a and $\mathrm{T}^{\pm}$ do not commute, taking the derivative in Eq. (22) requires the use of the Daletskii-Krein formula. Appendix B 2 explains the calculations involved in this process.

The run-and-turn model in $d = 3$ is treated along similar lines. Orientation is specified with polar and azimuthal angles (θ,ϕ) and can be handled with the spherical harmonic transform as described in Appendix A. The Liouvillian expression given in Eq. (19) still holds, with $\mathbf{u} = (\sin\theta\cos\phi, \sin\theta\sin\phi, \cos\theta)$ and Δ_a defined in Eq. (A6). In switching to transformed variables (l,m) for orientation, we exploit the properties of spherical harmonics [73]. The reorientation kernel involves convolution on the unit sphere, as previously used in the context of astrophysics [74–76].

B. Results: MSD and diffusivity

The method gives access to moments of any order, for arbitrary initial condition. We have obtained for instance the second moment when the initial orientation is fixed to a prescribed value θ_{in}. The resulting expression is lengthy and reported in Appendix D. In the following, we focus on the quantity of prime importance in experiments, the mean square displacement (MSD), denoted as $M(t)$. Two related quantities will also be discussed. First, the velocity correlation function, obtained by double differentiation $C(t) = M''(t)/2$, is particularly useful to emphasize the differences between patterns. Second, the diffusivity $\mathcal{D} = \lim_{t\to\infty} M'(t)/d$, also called diffusion coefficient or "random motility" [13], is the simplest characterization of a swimming pattern. Note that in terms of Laplace variable $C(s) = s^2 M(s)/2$ and $d\mathcal{D} = \lim_{s\to 0} C(s)$, and that $M(t) = d\langle x^2(t)\rangle$ if initial orientation is isotropically distributed.

The MSD and diffusivity for unimodal run-and-turn motion for arbitrary run time distribution $\psi(t)$ and dimension $d = 2$ or 3 are found to be

$$M(s) = \frac{2v^2}{\tau} \frac{1-\alpha-\tau s'+(-1+\alpha+\alpha\tau s')\psi(s')}{(ss')^2[-1+\alpha\psi(s')]}, \quad (23)$$

$$d\mathcal{D} = \frac{v^2}{\tau} \frac{1-\alpha-\tau \tilde{D}_\mathrm{r}+(-1+\alpha+\alpha\tau \tilde{D}_\mathrm{r})\psi(\tilde{D}_\mathrm{r})}{\tilde{D}_\mathrm{r}^2[-1+\alpha\psi(\tilde{D}_\mathrm{r})]}, \quad (24)$$

with τ the mean run time, $\tilde{D}_\mathrm{r} = (d-1)D_\mathrm{r}$, $s' = s + \tilde{D}_\mathrm{r}$, and $\alpha = \langle \cos\theta \rangle_h$, where $\langle . \rangle_h$ indicates an average over the turning angle distribution h. In contrast to the MSD that involves the whole function ψ, the diffusivity depends only on the quantity $\psi(\tilde{D}_\mathrm{r})$, explicitly given by [77]

$$\psi(\tilde{D}_\mathrm{r}) = \int_0^\infty dt\, e^{-(d-1)D_\mathrm{r}} \psi(t), \quad (25)$$

which is the average directional correlation at the end of a run. Here and in Eq. (24), the rotational diffusion is strictly nonzero $D_\mathrm{r} > 0$, as assumed in the following unless mentioned otherwise. As regards the turning angle, both the MSD and diffusivity depend only on the mean cosine, also called the persistence index [25], which is thus, rather than the mean turning angle, the relevant quantity [78].

For completeness, we also quote the MSD in nonsteady state

$$\frac{M_\mathrm{ns}(s)}{v^2} = \frac{1}{\tilde{D}_\mathrm{r} s^2 s'[1-\psi(s)][1-\alpha\psi(s')]} \times (\tilde{D}_\mathrm{r} - (s'-\alpha s)\psi(s) + [s - \alpha s' + \alpha \tilde{D}_\mathrm{r}\psi(s)]\psi(s')), \quad (26)$$

where $\tilde{D}_\mathrm{r}$ and s' are defined as in Eq. (23). Note that this result is different from the steady state expression. In the following, Eq. (26) will not be used, except in Sec. V B.

C. Alternative route to MSD

Before discussing its implications, we show how to recover the MSD for unimodal motion without having recourse to noncommutative calculus. Again we consider only the case $d = 2$ for simplicity and start with the orientation correlation function

$$C_\mathrm{or}(t-t') = \langle \mathbf{u}(t)\cdot\mathbf{u}(t') \rangle = \langle \cos[\theta(t)-\theta(t')] \rangle, \quad (27)$$

which is simply $C(t)/v^2$ since the velocity modulus is constant. C_or can be obtained from the expression

$$C_\mathrm{or}(t) = \int_{-\pi}^{\pi} d\theta\, P(\theta,t)\cos\theta, \quad (28)$$

where $P(\theta,t)$ is the probability density of orientation θ at time t, given the initial state $P_\mathrm{in}(\theta) = \delta(\theta)$. Switching to transformed variables, Eq. (28) translates into

$$C_\mathrm{or}(s) = \pi[P(l=1,s) + P(l=-1,s)]. \quad (29)$$

Next we use the generic formalism of Sec. II A to determine $P(l,s)$. The continuous evolution of orientation involves only rotational diffusion, implying $\mathcal{L} = D_\mathrm{r}\partial^2_{\theta\theta}$ in θ variable and $\mathcal{L} = -D_\mathrm{r} l^2$ in Fourier series variable l. With the initial orientation $P_\mathrm{in}(l) = 1/2\pi$, applying Eq. (7) leads to

$$P(l,s) = \left[\psi_\chi(\hat{\mathcal{L}}) + \frac{2\pi h(l)\psi_\alpha(\hat{\mathcal{L}})\psi_\beta(\hat{\mathcal{L}})}{1-2\pi h(l)\psi(\hat{\mathcal{L}})}\right]\frac{1}{2\pi}, \quad (30)$$

with $\hat{\mathcal{L}} = s - \mathcal{L} = s + D_\mathrm{r} l^2$. Here, all "operators" involve only multiplication with respect to the l variable and therefore commute. Combining Eqs. (29) and (30) yields an explicit expression for $C_\mathrm{or}(s)$. Using finally $M(s) = 2v^2/s^2 \times C_\mathrm{or}(s)$ gives back Eq. (23) for the MSD. Though it cannot address higher moments, or even the second moment with fixed initial orientation, this method is simple and provides one way to validate the more involved noncommutative route. Further checks were also conducted, including comparison with literature results and numerical simulations, as well as an alternative approach to obtain arbitrary moments in the Poissonian case. They are gathered in Appendix C.

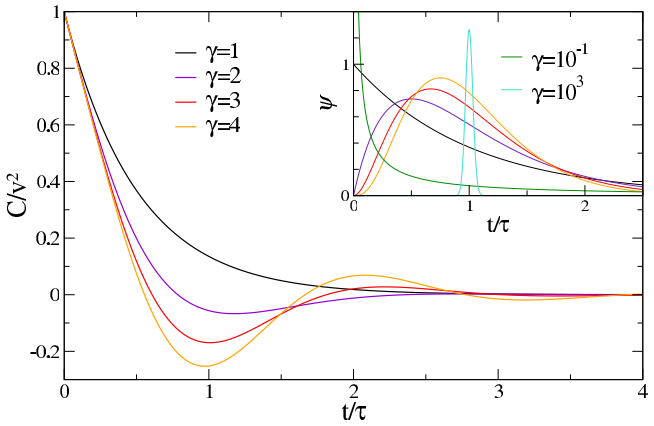

FIG. 3. Velocity correlation function for unimodal run-reverse motion with vanishing D_r and a gamma distribution of run time. The latter, with mean τ and parameter γ, is shown in the inset. The curve with $\gamma = 10^3$ is rescaled for clarity.

D. Applications

1. Run-reverse and minimum in C(t)

As a first application, we consider a simple instance of run-reverse pattern. To do so, let us introduce a particular choice of run time that will be used repeatedly in this work, the gamma distribution, defined as

$$\psi(t) = \frac{t^{\gamma-1}e^{-\gamma t/\tau}}{\Gamma(\gamma)(\tau/\gamma)^\gamma}, \quad \psi(s) = \left[1+\frac{\tau s}{\gamma}\right]^{-\gamma}, \quad (31)$$

where Γ is the gamma function and $\gamma > 0$ is the only parameter once the mean run time τ is fixed. Already used to fit experimental data [8,42,70], the gamma distribution includes the Poissonian case when $\gamma = 1$, and exhibits a maximum followed by an exponential tail for $\gamma > 1$, as visible in the inset of Fig. 3. Note that choosing an integer γ yields an Erlang distribution, for which the run time is the sum of γ independent exponentially distributed variables with mean τ/γ [79]. Besides, the limit $\gamma \to 0$ yields a power law regime with $\psi(t) \sim t^{-1}$, ending with an exponential cutoff. In the

opposite limit $\gamma \to \infty$, $\psi(t)$ approaches a Gaussian with vanishing variance, and turning events become quasiperiodic.

The run-reverse pattern is assumed to have identical characteristics in the forward and backward motions, and can then be described as a unimodal run-and-turn with $\alpha = -1$. With run times that are gamma distributed, one can obtain for the velocity correlation function an expression valid for all values of γ,

$$\frac{C(t)}{v^2} = e^{-\tilde{D}_r t}\Big[1 - 2t + 4\gamma^\gamma \times \int_0^t dt'(t-t')t'^{\gamma-1}e^{-\gamma t'}E_{\gamma,\gamma}[-(\gamma t')^\gamma]\Big], \quad (32)$$

where E_{μ_1,μ_2} is the two-parameter Mittag-Leffler function [80]. As a side remark, note that the effect of rotational diffusion is limited to the exponential term that comes as a prefactor, a conclusion that actually holds for any unimodal motion since $C(s)$ depends only on $s' = s + \tilde{D}_r$. For the first integer values of γ, Eq. (32) reduces to compact expressions involving only elementary functions. With the notation $a = 2\sqrt{2}$, they read as [81]

$$C(t) = v^2 e^{-\tilde{D}_r t} f_\gamma(t/\tau), \quad (33)$$

$$\gamma = 1, \quad f_1(t) = e^{-2t},$$

$$\gamma = 2, \quad f_2(t) = e^{-2t}\cos(2t),$$

$$\gamma = 3, \quad f_3(t) = \frac{e^{-6t}}{9}[1 + 8e^{9t/2}\cos(3\sqrt{3}t/2)],$$

$$\gamma = 4, \quad f_4(t) = e^{-4t}\cos(at)\Big[\cosh(at) + \frac{a}{4}\sinh(at)\Big].$$

In the Poissonian case, the velocity correlation function for unimodal motion is an exponential for all values of D_r and α, thus decreasing monotonically to zero. The non-Poissonian case can be qualitatively different, as illustrated in Fig. 3 for vanishing D_r. Upon increasing γ above unity, the velocity correlation functions exhibit in the vicinity of τ an increasingly pronounced minimum, whose negative value is the sign of anticorrelation. Even though only the first minimum is clearly visible, there is actually a sequence of alternating minima and maxima [82]. Interestingly, a negative minimum in $C(t)$ has been reported twice recently: first, in the orientation correlation function of *P. putida* [8], whose pattern is unimodal when considering only the direction of motion and not its velocity, and second, in the context of cell motility, for the velocity autocorrelation of *Dictyostelium discoideum* amoeba [83]. Within the unimodal run-and-turn model, such nonmonotonicity can arise only if the turning process is not Poissonian [84].

The existence of a minimum in $C(t)$ is not restricted to perfect reversal ($\alpha = -1$) but may arise if α is negative. The minimum will be most noticeable for low α, low D_r, and high γ, when the turning process involves a more pronounced memory. Shown in Fig. 4 is the minimal value, computed numerically as a function of $\tilde{D}_r$ for the first integer values of γ and $\alpha = -1$, $-3/4$, and $-1/2$. While the minimum may reach -0.25, its typical value is around -0.1 for $\gamma = 3$, $\alpha = -3/4$, and $\tau\tilde{D}_r = 0.1$. When the effect of rotational diffusion becomes significant ($\tau\tilde{D}_r \simeq 1$), the minimum magnitude declines to a level that may be difficult to detect experimentally.

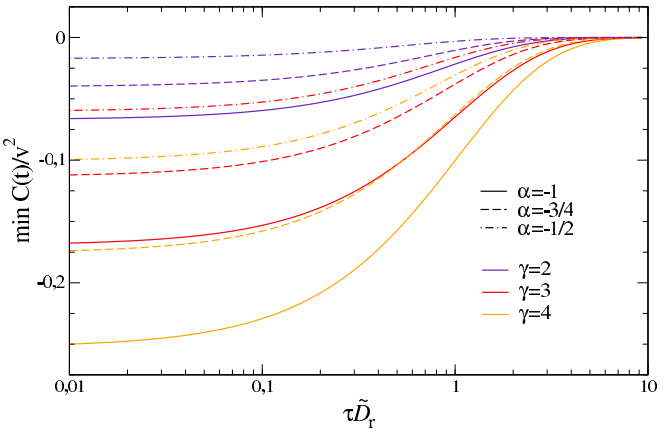

FIG. 4. Minimum value in velocity correlation function $C(t)/v^2$, as a function of rotational diffusion $\tilde{D}_r = (d-1)D_r$. The run time is gamma distributed with mean τ and parameter γ.

2. *Maximizing the diffusivity*

As it characterizes the exploratory behavior in a homogeneous environment, the diffusivity is a basic feature of a swimming pattern. Can it be maximized with a particular choice of parameters? It is intuitively expected that turning events that are more persistent lead to higher diffusivity. It can be checked from Eq. (24) that $\mathcal{D}$ is indeed monotonically increasing with α. In contrast, the dependence on rotational diffusion coefficient is not always monotonic: diffusivity may reach a maximum at a finite value of D_r, as pointed out recently in the particular case of the run-reverse pattern [70]. We are now in a position to complete the picture for a generic unimodal motion.

We first present a criterion for the existence of a maximum, valid for any run time distribution. Keeping τ fixed, we introduce the dimensionless diffusivity

$$\bar{\mathcal{D}} = \frac{2d\mathcal{D}}{v^2\tau}, \quad (34)$$

which allows us to treat simultaneously the cases $d = 2$ and 3. In the limit of large rotational diffusion $D_r \to \infty$, $\bar{\mathcal{D}}$ approaches $2/(\tau\tilde{D}_r)$ and is thus always decreasing. If the slope is positive at low D_r, then a maximum must exist in between. This sufficient condition can be recast as

$$\frac{\mu_3}{\tau^3} \leqslant -\frac{3(1+\alpha)}{1-\alpha}\frac{\sigma^2}{\tau^2} - \frac{1+\alpha(4+\alpha)}{(1-\alpha)^2}, \quad (35)$$

where σ^2 is the variance of the run time distribution, and $\mu_3 = \int_0^\infty dt\,(t-\tau)^3\psi(t)$ is its third central moment [85].

To make further progress, let us now consider a gamma distribution of run time. The dimensionless diffusivity is plotted in Fig. 5 as a function of rotational diffusion, for a run-reverse motion. While the curves are strictly decreasing at low γ, they exhibit a maximum for higher values. For $\alpha = -1$, the transition between those two regimes occurs at a critical value $\gamma_c = 2$. For incomplete reversal ($\alpha > -1$), the transition can also be seen for sufficiently low α, but γ_c rapidly increases

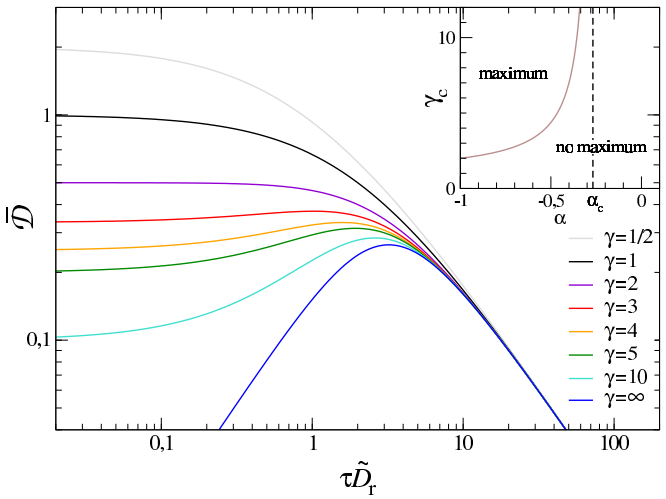

FIG. 5. Dimensionless diffusivity as a function of rotational diffusion coefficient for a run-reverse pattern ($\alpha = -1$), and gamma distributed run time. There is a maximum for $\gamma \geqslant \gamma_c = 2$. Inset: critical value $\gamma_c(\alpha)$ above which a maximum exists.

with α, as shown in the inset of Fig. 5 [86]. Eventually, for $\alpha \geqslant \alpha_c = -2 + \sqrt{3}$, even periodic turning ($\alpha = \infty$) does not yield a maximum. The (α,γ) plane is thus divided in two regions, with or without a maximum. Schematically, the maximum arises when turning event occurs at the right time to counteract the change in orientation imparted by rotational diffusion. This effect is most pronounced when reversals are sharp and the turning process close to periodic.

Figure 6 displays the maximal diffusivity $\bar{\mathcal{D}}^*$, and the optimal rotational diffusion coefficient $\tilde{D}_r^*$ at which it is reached, with $\tilde{D}_r^*$ finite when a maximum exists and zero otherwise. Numerically, $\tau\tilde{D}_r^*$ is of order unity for perfect reversal ($\alpha = -1$) but much lower values may also be optimal when reversal is only partial: for instance, $\tau\tilde{D}_r^* \simeq 0.1$ for $\gamma = 3$ and $\alpha \simeq -0.68$ or for $\gamma = 5$ and $\alpha \simeq -0.48$. As regards $\bar{\mathcal{D}}^*$, it evolves continuously at the transition between the two regimes and increases steadily with α as explained above. Note that for $\alpha \to 1$, $\bar{\mathcal{D}}^*$ diverges as $2/(1-\alpha)$, because with $\tilde{D}_r = 0$, motion becomes ballistic rather than diffusive.

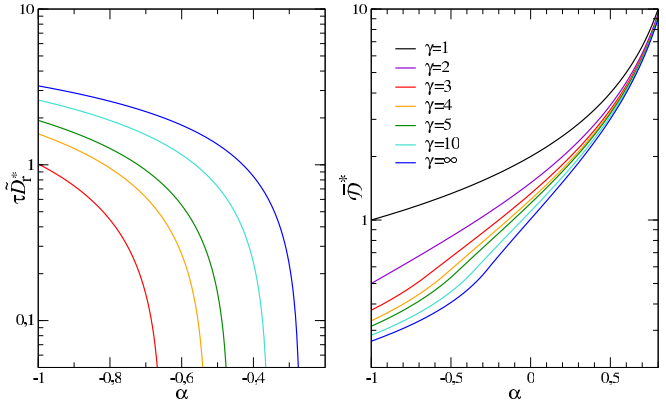

FIG. 6. Optimal rotational diffusion coefficient $\tilde{D}_r^*$ (left) and maximal diffusivity $\bar{\mathcal{D}}^*$ (right), as a function of α for gamma distributed run time.

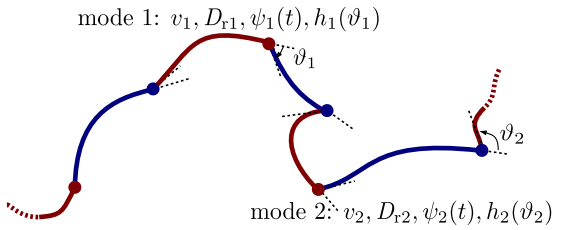

FIG. 7. Model of bimodal run-and-turn motion. Two modes alternate, whose parameter sets are different.

As a final remark, we point out that the diffusivity, at maximum or not, and for any α, is a strictly decreasing function of the γ parameter. This is visible in Figs. 5 and 6 and can be checked analytically. As a result, periodic turning yields the lowest diffusivity, and the highest value is reached for $\gamma \to 0$. In this limit, $\psi(t)$ develops a t^{-1} tail, the motion is dominated by long runs, and the effect of turns becomes negligible with respect to rotational diffusion, leading to $d\mathcal{D} = v^2/\tilde{D}_r$. This limiting case may be relevant, since a power law in run time distribution has been observed in *E. coli* [48], whose exponent 1.2 is close to unity. Finally, note that among gamma distributions that remain finite ($\gamma \geqslant 1$), the Poissonian case $\gamma = 1$ yields the highest diffusivity.

IV. BIMODAL RUN-AND-TURN

A. Model and MSD

Most swimming patterns feature more than a single type of runs or turning events. The most common case involves a binary alternation in one or several parameters. This may be the velocity modulus as in *R. sphaeroides* [87] or *P. putida* [8,44], the turning angle as in the run-reverse-flick pattern of *V. alginolyticus* [7], or the mean run time as in *C. crescentus* [45]. The description of such patterns requires a bimodal extension of the run-and-turn model, where two modes $i = 1,2$ alternate, each with its own run time distribution ψ_i and mean τ_i, velocity v_i, rotational diffusion coefficient D_{ri}, and reorientation kernel h_i (Fig. 7).

The operator formalism is easily generalized to bimodal evolution. Retracing the steps of Sec. II A, one obtains the system

$$J_1(\mathbf{q},s) = h_2(\mathbf{q})\psi_2(\hat{\mathcal{L}}_2)J_2(\mathbf{q},s) + h_2(\mathbf{q})\psi_{\alpha 2}(\hat{\mathcal{L}}_2)P_{\text{in},2}(\mathbf{q}), \quad (36)$$

$$P_1(\mathbf{q},s) = \psi_{\beta 1}(\hat{\mathcal{L}}_1)J_1(\mathbf{q},s) + \psi_{\chi 1}(\hat{\mathcal{L}}_1)P_{\text{in},1}(\mathbf{q}), \quad (37)$$

where all quantities are defined for each mode 1 and 2, and with the convention that within a mode, the jump occurs after the run [88]. The generating function for the total probability density $P = P_1 + P_2$ is

$$P(\mathbf{q},s) = [\hat{\chi}_1 + \hat{\beta}_2(1-\hat{\sigma}_1\hat{\sigma}_2)^{-1}\hat{\alpha}_1 + \hat{\beta}_1\hat{\sigma}_2(1-\hat{\sigma}_1\hat{\sigma}_2)^{-1}\hat{\alpha}_1]P_{\text{in},1}(\mathbf{q}) + S_{1\leftrightarrow 2}. \quad (38)$$

Here, $S_{1\leftrightarrow 2}$ indicates that everything preceding the symbol is repeated with indices 1 and 2 interchanged, and dependence on $(\mathbf{q},s)$ is implicit for the operators $\hat{\sigma}_i = h_i(\mathbf{q})\,\psi_i(\hat{\mathcal{L}}_i)$,

$\hat{\alpha}_i = h_i(\mathbf{q})\,\psi_{\alpha i}(\hat{\mathcal{L}}_i)$, $\hat{\beta}_i = \psi_{\beta i}(\hat{\mathcal{L}}_i)$, $\hat{\chi}_i = \psi_{\chi i}(\hat{\mathcal{L}}_i)$, where $\hat{\mathcal{L}}_i = s - \mathcal{L}_i$ and $i = 1,2$. Applying Eq. (38) to the bimodal run-and-turn model, we obtain our main result, the general expression for the MSD in terms of Laplace variable. With the notations $s_i = s + (d-1)D_{ri}$, $\Psi_i = \psi_i(s_i)$, $d = 2$ or 3, and $\alpha_i = \langle \cos\theta \rangle_{h_i}$, it reads as

$$\frac{M(s)}{2} = \frac{v_1^2 s_2^2[\tau_1 s_1(1-\alpha_1\alpha_2\Psi_1\Psi_2) - (1-\Psi_1)(1-\alpha_1\alpha_2\Psi_2)] + S_{1\leftrightarrow 2} + v_1 v_2(\alpha_1+\alpha_2)s_1 s_2(1-\Psi_1)(1-\Psi_2)}{(\tau_1+\tau_2)(s\,s_1\,s_2)^2(1-\alpha_1\alpha_2\Psi_1\Psi_2)}. \tag{39}$$

B. Applications

1. Individual patterns

The bimodal run-and-turn model includes as particular cases all swimming patterns observed so far. Here we illustrate some concrete examples and discuss some consequences of the general expression Eq. (39). Throughout this section, Sec. IV B, we focus on the three-dimensional case, which is most relevant for freely swimming bacteria.

Run-and-tumble or run-stop. The unimodal run-and-turn model assumes that turning events are instantaneous. This approximation, however, is not obvious, as there is no clear separation of time scale. The average run and tumble times in *E. coli* are $\tau_1 = 0.86$ s and $\tau_2 = 0.14$ s, respectively [5], yielding $\tau_1/\tau_2 \simeq 6$. The ratio for *R. sphaeroides* reaches even smaller values, as low as 3 [89]. Therefore, it seems warranted to investigate a more refined model that accounts for the finite duration of tumble or stopping mode. To do so, we consider a bimodal pattern with no turning event, a mode 1 for the runs, and a mode 2 which describes explicitly a reorientation governed by active rotational diffusion with coefficient $D_{r2} > D_{r1}$, as relevant for *E. coli* and *R. sphaeroides* [14,87]. Choosing run times that are exponentially distributed, one can obtain an explicit expression for $C(t)$ which is reported in Eq. (D3), and that we use with $v_2 = 0$, assuming velocity during reorientation is negligible.

We now compare the predictions of this bimodal model to those of an equivalent unimodal model with instantaneous turning events. For the latter, $D_r = D_{r1}$, $\tau = \tau_1$, and the α parameter is chosen equal to the mean cosine of angle change at the end of reorientation mode 2, leading to $\alpha = 1/(1 + 2\tau_2 D_{r2})$ [90]. Taking typical values for D_{r1} and D_{r2} in *E. coli* [91], it turns out that the normalized velocity correlation functions $C(t)/\langle v^2 \rangle$ predicted by the unimodal and bimodal models are very close to each other (not shown). The maximal absolute deviation never exceeds 0.05, whenever $D_{r2}/D_{r1} \geqslant 10$ and even for τ_1/τ_2 reaching unity. From this result, it is understandable why tumbles whose duration is not negligible can nevertheless be approximated as instantaneous.

Two-velocity run-reverse. In the swimming pattern of *P. putida*, the average velocity varies by a factor of 2 between the forward and backward modes. Let us fix $v_1 = 2v_2 = v$ and for simplicity, assume that all other parameters are identical in the two modes, $D_{r1} = D_{r2} = D_r, \tau_1 = \tau_2 = \tau, \alpha_1 = \alpha_2 = -1$. Choosing for both modes a gamma distributed run time with $\gamma_1 = \gamma_2 = 2$ is consistent with experimental data [8] and yields the very compact formula

$$\frac{C(t)}{v^2} = \frac{e^{-2D_r t}}{16}[1 + 9e^{-2t/\tau}\cos(2t/\tau)]. \tag{40}$$

As can be seen in Fig. 8, $C(t)$ at sufficiently low D_r exhibits a minimum, followed by a plateau and a gentle decay to zero [92]. Note that in contrast with the unimodal run-reverse pattern (Fig. 3), the minimum value is positive. The characteristic shape of $C(t)$ had been noticed previously using numerical simulation [8], it can now be described analytically.

Run-reverse-flick. To limit the number of parameters, we again set $v_1 = v_2 = v$, $D_{r1} = D_{r2} = D_r$, and $\alpha_1 = -1$, $\alpha_2 = 0$, and take a gamma distribution of run time with $\gamma_1 = \gamma_2 = 2$. The latter is the simplest choice that allows us to capture both a maximum and an exponential tail, as observed for *C. crescentus* and *V. alginolyticus*. In the former, the forward and backward swimming time are widely different [45,93]. The velocity correlation function in this case is lengthy and given in Eq. (D4). On the other hand, assuming the same mean run time $\tau_1 = \tau_2 = \tau$, which would be a reasonable approximation for *V. alginolyticus* [43], one gets the very concise expression

$$\frac{C(t)}{v^2} = e^{-(2D_r + 2/\tau)t}\left[-\frac{t^3}{3\tau^3} - \frac{t^2}{\tau^2} + \frac{t}{2\tau} + 1\right]. \tag{41}$$

Having considered each swimming pattern individually, we finally examine to which extent they differ in their velocity correlation functions. Those are plotted in Fig. 8 for the four types considered so far: run-and-tumble, one- and two-velocity run-reverse, and run-reverse-flick. For comparison, a single mean run time τ is assumed everywhere. For each pattern, the Poissonian pattern ($\gamma = 1$) is shown, along with the simplest instance of non-Poissonian case ($\gamma = 2$). Simple analytical expressions, such as Eqs. (40) and (41), are available for all curves. Interestingly, it is possible to identify features that

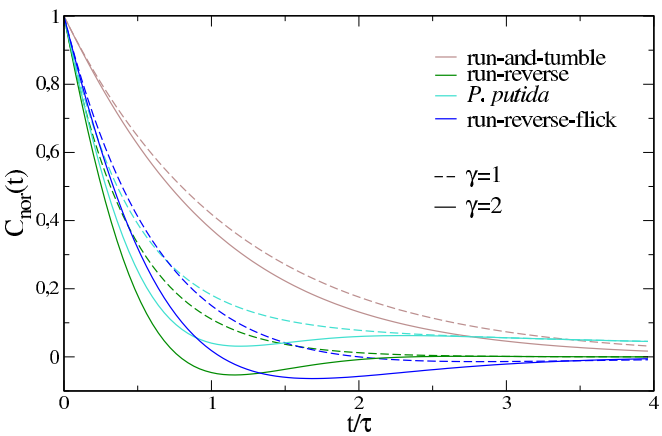

FIG. 8. Normalized velocity correlation function $C_{\rm nor}(t) = C(t)/\langle v^2 \rangle$ for four types of swimming patterns. The run time is gamma distributed with $\gamma = 1$ (Poissonian case) or $\gamma = 2$ and has the same mean τ in all modes. For the run-and-tumble, $\alpha = 0.33$ as in *E. coli*. The rotational diffusion coefficient is $\tau D_r = 0.1$.

discriminate between patterns: the monotonic decay of run-and-tumble, the positive plateau at intermediate time for *P. putida*, and in the non-Poissonian case, the negative minimum when a full reversal is involved, with a different location in time for run-reverse and run-reverse-flick. The deviation between curves is more pronounced in the non-Poissonian case. Note also that rotational diffusion in Fig. 8 is set to a typical order of magnitude $\tau D_r = 0.1$. The differences between curves are more noticeable for lower D_r, but gradually vanish for higher values, as the decorrelation in orientation during runs comes to dominate the effect of turning events. Overall, the velocity correlation function may prove a useful quantity for pattern identification: an accurate measurement can provide a first insight into the type of underlying pattern.

2. *Diffusivity: Bimodal vs unimodal*

What are the benefits of a bimodal pattern? Given the number of parameters, including a function for the run time distribution, it seems unlikely that a general statement can be made. Here we show that some conclusions may be drawn when focusing on diffusivity. To do so, we compare bimodal and unimodal patterns having identical properties, except for one parameter that differs in mode 1 and mode 2 of bimodal motion, and is set to the mean value in the unimodal process, so that the "average" properties are the same. For the two patterns thus defined, we consider the ratio of diffusivities $\mathcal{R} = \mathcal{D}_{\rm bim}/\mathcal{D}_{\rm uni}$.

Let us start with bimodality in angle, for which $\alpha_1 \neq \alpha_2$ and $\alpha_m = (\alpha_1 + \alpha_2)/2$ in the bimodal and unimodal cases respectively. In the limit of vanishing rotational diffusion, which corresponds to straight runs, the result takes a very tractable form,

$$\mathcal{R} = 1 - \frac{(\alpha_1 - \alpha_2)^2}{2(1 - \alpha_1\alpha_2)[1 + \alpha_m + (1 - \alpha_m)\sigma^2/\tau^2]}, \quad (42)$$

valid for any run time distribution with finite variance σ^2. It is clear from Eq. (42) that the bimodal pattern has lower diffusivity. When rotational diffusion is finite, the expression for $\mathcal{R}$ is more involved, and accordingly, we assume again a gamma distribution of run time. It turns out that $\mathcal{R} \leqslant 1$ for any γ, indicating that bimodality in angle reduces diffusivity.

Addressing now bimodality in velocity, we fix $v_1 \neq v_2$ and $v_m = (v_1 + v_2)/2$ for the bimodal and unimodal processes respectively. In the absence of rotational diffusion,

$$\mathcal{R} = 1 + \frac{(v_1 - v_2)^2}{4{v_m}^2} \frac{\sigma^2/\tau^2 + \kappa}{\sigma^2/\tau^2 + \kappa^{-1}}, \quad \kappa = \frac{1 - \alpha}{1 + \alpha}, \quad (43)$$

which, this time, is always above unity. For gamma distributed run time, this conclusion also applies with finite D_r, indicating that bimodality in velocity enhances diffusivity.

Plotted in Fig. 9 is the diffusivity ratio for bimodality in angle and velocity, with the choice $\gamma = 2$ and $\tau D_r = 0.1$, a typical order of magnitude. For concreteness, let us take two examples. Compared to a unimodal pattern with $\alpha = -1/2$, the run-reverse-flick has a lower diffusivity ($\mathcal{R} = 0.7$). In contrast, with respect to a unimodal motion with the same average velocity, the two-velocity run-reverse of *P. putida* has a diffusivity which is three times higher ($\mathcal{R} = 3.2$). The influence of γ and D_r on $\mathcal{R}$ is shown in Fig. 10, for

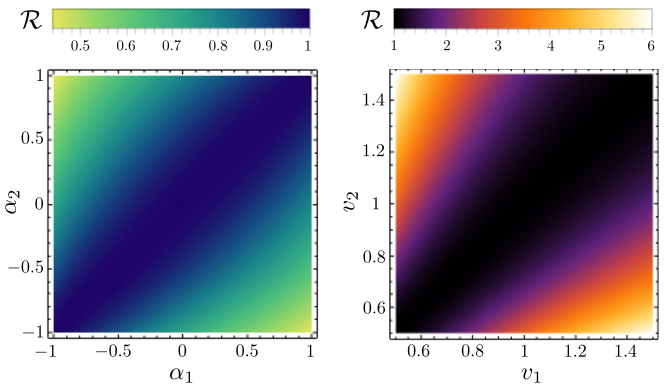

FIG. 9. Diffusivity ratio $\mathcal{R}$ between bimodal and unimodal motions, for bimodality in angle (left) and velocity (right). In the latter, the pattern is run-reverse ($\alpha = -1$). In both cases, $d = 3$, $\tau D_r = 0.1$, and $\gamma = 2$.

the run-reverse-flick and the two-velocity run-reverse with $v_1/v_2 = 2$ as in *P. putida*. In both cases, the deviation from unity is increasingly pronounced with γ, and would be maximal for periodic turning. For the run-reverse-flick, the $\mathcal{R}$ ratio is an increasing function of rotational diffusion, with minimal value $\mathcal{R} = 3/(3 + \gamma)$ at vanishing D_r, and which approaches unity when $\tau D_r \gtrsim 1$. The diffusivity enhancement for the two-velocity run-reverse increases upon reducing D_r, and diverges as $\mathcal{R} \sim \gamma/D_r$ for γ finite and $D_r \to 0$, because the bimodal motion then becomes ballistic. Unless rotational diffusion dominates ($\tau D_r \gtrsim 1$), the enhancement in diffusivity is very significant.

V. EXTENSIONS

A. Curved runs

Intrinsically curved trajectories arise naturally for bacteria in the presence of solid interfaces. Hydrodynamic interactions attract bacteria to the vicinity of the surface, where they swim with parallel orientation and circular trajectories [94,95]. With reorientations occurring mostly parallel to the wall and turning events reduced in frequency, bacteria may remain trapped [96]. Circular trajectories are also relevant for a variety of systems, including magnetotactic bacteria in rotating magnetic field [97], asymmetric artificial microswimmers [98,99], or the gliding of diatom *Nitzschia communis* [100].

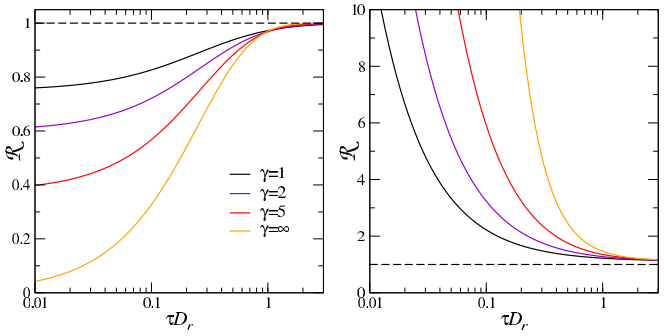

FIG. 10. Diffusivity ratio $\mathcal{R}$ as a function of rotational diffusion, for the run-reverse-flick pattern (left) and the two-velocity run-reverse with $v_1/v_2 = 2$ (right).

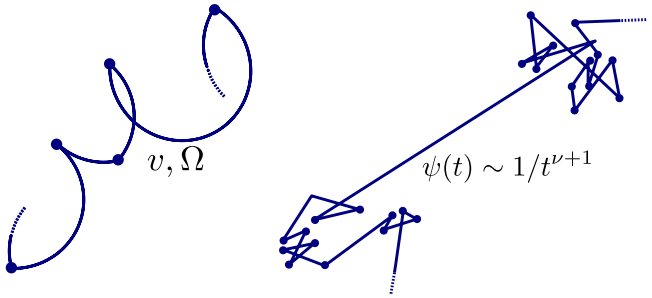

FIG. 11. Two extensions of the run-and-turn model. Left: Curved runs with constant mean curvature Ω. In the absence of rotational diffusion, trajectories are circular. Right: Lévy walks, in which motion is ballistic with a heavy tail in the distribution of run time.

We consider here the simplest case of run-and-turn motion with curved runs: a unimodal model with constant mean curvature in dimension $d = 2$ (Fig. 11). It is straightforward to extend the approach of Sec. III: the Liouvillian of Eq. (19) now includes an additional drift term $-\Omega\,\partial_\theta p$, where Ω is the angular velocity. If interested only in the diffusivity, one can use the method of Sec. III C. The final result is

$$\frac{4\mathcal{D}}{v^2\tau} = \frac{1}{(\tau\xi)^2}\left[\tau\xi - 1 + \psi(\xi) + \frac{\alpha(1-\psi(\xi))^2}{1-\alpha\psi(\xi)}\right] + \text{c.c.}, \quad (44)$$

where $\psi(\xi) = \psi(s = \xi)$, $\xi = D_r - i\Omega$, c.c. is the complex conjugate, and $\mathcal{D}$ is an even function of Ω as required. In the particular case of Poissonian isotropic turns and circular runs (ψ exponential, $\alpha = 0$, $D_r = 0$), this expression reduces to that of Ref. [39]. In the absence of turns ($\alpha = 1$), one recovers the expression found previously [98,101,102].

Let us examine the consequences of Eq. (44) for a gamma distribution of run time, considering first the limit of vanishing rotational diffusion. The diffusivity as a function of angular velocity Ω is displayed in Fig. 12, for turning events that are perfect reversals ($\alpha = -1$). Two regimes may be distinguished. In the first, $\mathcal{D}(\Omega)$ reaches a single maximum at $\Omega^* = 0$, implying that compared to curved ones, straight runs always yield a higher diffusivity. In the second regime, $\mathcal{D}(\Omega)$ exhibits two symmetric maxima at an optimal value of angular velocity $\pm\Omega^* \neq 0$. In this situation, the changes in orientation occurring during the run and during the turn compensate each other to some extent, making the decorrelation in orientation slower [103].

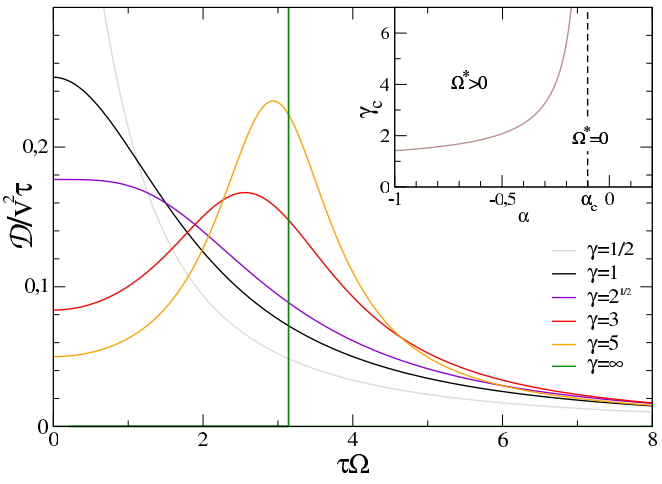

FIG. 12. Diffusivity as a function of angular velocity for a two-dimensional unimodal run-reverse with curved runs. Run time is gamma distributed with parameter γ and $D_r = 0$. Inset: diffusivity is maximized by a finite angular velocity Ω^* when $\gamma > \gamma_c(\alpha)$.

To delineate the boundary between the two regimes, we observe that $\mathcal{D}(\Omega)$ decreases as Ω^{-2} at large Ω and has zero slope at the origin. Therefore, a sufficient condition for the existence of two maxima is that the second derivative at the origin is positive. In the case $\alpha = -1$, this criterion translates into $\gamma > \gamma_c = \sqrt{2}$ [104]. The second regime may also be found for incomplete reversal if $\gamma > \gamma_c(\alpha)$, where $\gamma_c(\alpha)$, the solution of a third order polynomial, is plotted in the inset of Fig. 12. Note that the increase of $\gamma_c(\alpha)$ at low α is weak, since for α up to -0.33, it remains below 3. The second regime disappears for $\alpha > \alpha_c = -5 + 2\sqrt{6} \simeq -0.101$. In that case, even periodic turning would not yield a maximum at finite Ω^* and straight runs always lead to faster spreading.

The picture that applies at $D_r = 0$ remains valid to a large extent at low τD_r. As a quantitative measure, consider for instance $\alpha_c(\tau D_r)$, whose values show only modest variation: -0.101, -0.107, and -0.17 for $\tau D_r = 0$, 0.1 and 1 respectively. Eventually, for very strong rotational diffusion ($\tau D_r > 5.54$), the spread in orientation prevents the compensation mechanism between angular velocity and turning events, and only the first regime survives. As regards the maximal value of diffusivity (not shown), we note that for $\gamma \geqslant 1$, the Poissonian case generally yields the highest diffusivity, except at low α, low D_r and high γ.

We have focused on the unimodal model for simplicity. Bimodality in curvature has been considered theoretically, with a dichotomous switching of curvature [105,106], and has been reported in diatom *N. communis*, whose curvature is constant in absolute value, but alternates in sign [100]. This situation can be handled in the present formalism with a bimodal model.

B. Ballistic runs and Lévy walks

In this final section, we take a step aside from bacterial motions and focus on Lévy walks by considering ballistic runs whose distribution is fat-tailed (Fig. 11). Even though power laws have been observed in *E. coli* [48], they would not yield anomalous behavior, because the rotational diffusion, which is never strictly zero for bacteria due to thermal fluctuations, dominates at long time and leads to normal diffusion. If not relevant for the swimming of a single bacterium, Lévy walks have been shown recently to provide an adequate description for bacterial motion in densely packed swarms of millions of individuals that exhibit large-scale swirling [107]. More generally, Lévy walks are relevant in a variety of fields, from condensed matter to biophysics and behavioral ecology [108]. Yet, as pointed out recently [71], most investigations have focused primarily on the one-dimensional case. Here, as a straightforward application of our generalized run-and-turn model, we consider Lévy walks in dimensions $d = 2$ and $d = 3$, and with turning events that, in contrast to the traditional assumption, are not necessarily isotropic but may be arbitrary. We find that in spite of this generalization, the essential properties remain those of one-dimensional Lévy walks.

Let us start with the general expression for the MSD when runs are ballistic ($D_r = 0$),

$$M(s) = \frac{2v^2}{\tau s^4}\frac{1-\alpha-\tau s+(-1+\alpha+\alpha\tau s)\psi(s)}{-1+\alpha\psi(s)}, \quad (45)$$

$$M_{\rm ns}(s) = \frac{2v^2}{s^3}\left[1+\frac{(1-\alpha)s\psi'(s)}{[1-\psi(s)][1-\alpha\psi(s)]}\right], \quad (46)$$

in the steady and nonsteady case respectively. For the particular case of isotropic turns ($\alpha = 0$), Eq. (45) is in agreement with the results of Ref. [55], and Eq. (46) is consistent with those of Ref. [54]. Whenever the run time distribution has finite variance σ^2, a small-s expansion gives $\psi(s) = 1 - \tau s + (\tau^2 + \sigma^2)s^2/2 + O(s^3)$ and using Tauberian theorems, the long-time behavior is normal diffusion [109]

$$M(t) = v^2\tau\left[\frac{\sigma^2}{\tau^2}+\frac{1+\alpha}{1-\alpha}\right]t, \quad (47)$$

with a diffusivity that, unlike the case $D_r > 0$, involves only the mean and variance rather than the whole function $\psi(t)$.

We now consider a power law distribution of run time $\psi(t) \sim 1/t^{\nu+1}$ with $1 < \nu < 2$. The mean value τ is defined but the variance is infinite. In a small-s expansion, the fat tail results in a term with noninteger exponent

$$\psi(s) = 1 - \tau s + c(\tau s)^\nu + O(s^3). \quad (48)$$

For instance, two specific examples that have often been used are

$$\psi_I(t) = \frac{\nu/t_o}{(1+t/t_o)^{1+\nu}}, \quad \psi_{II}(t) = \frac{\nu t_o^\nu}{t^{1+\nu}}H(t-t_o), \quad (49)$$

where H is the Heaviside function and in which cases, $\tau_I = t_o/(\nu-1)$ and $c_I = -(\nu-1)^\nu\Gamma(1-\nu)$, $\tau_{II} = \nu\tau_I$ and $c_{II} = \nu^{-\nu}c_I$. If Eq. (48) holds, the long-time behavior is superdiffusive with

$$\frac{M(t)}{v^2\tau^2} = \frac{2c}{\Gamma(4-\nu)}\left(\frac{t}{\tau}\right)^{3-\nu}. \quad (50)$$

In agreement with Ref. [41], which relies on a different computation, we see that the distribution of turning angle plays no role. This is consistent with the intuitive picture that motion is dominated by the longest run. Equation (50) is valid for the steady case only. With the nonsteady assumption, the asymptotic behavior is different and, whatever the value of c, reads as

$$M_{\rm ns}(t) = (\nu-1)M(t). \quad (51)$$

Several remarks are in order. First, for the particular choice $\psi = \psi_I$, $d = 2$ and nonsteady assumption, one recovers the results of Ref. [71] which investigates several instances of two-dimensional Lévy walks. The product, XY, or uniform model all have $\alpha = 0$. For a generic run-and-turn motion [see Eq. (23)], this is sufficient to ensure an identical MSD [110]. With Lévy walks, the actual value of α is irrelevant. Second, one way to characterize the ergodicity properties is to introduce the ergodicity breaking parameter $\mathcal{EB}(t) = M_T(t)/M_{\rm ns}(t)$, where $M_T(t) = \langle\overline{\mathbf{r}^2}(t,T)\rangle$, and $\overline{\mathbf{r}^2}(t,T) = (T-t)^{-1}\int_0^{T-t}dt'\,[\mathbf{r}(t'+t)-\mathbf{r}(t')]^2$ denotes the time average taken over the whole trajectory duration T. In the limit of long time, $M_T(t)$ approaches the steady state value and Eq. (51) can be rewritten as

$$\lim_{t\to\infty}\mathcal{EB}(t) = \frac{1}{\nu-1}, \quad (52)$$

which differs from unity, except in the case $\nu \to 2$ where standard diffusion is recovered. Thus, even though the mean time is finite, the steady and nonsteady MSDs are distinct in the long time limit. However, they do so only by a prefactor. This is the ultraweak ergodicity breaking discussed for the one-dimensional case [111,112]. It turns out that this feature carries over to higher dimensions, and for arbitrary turning angle distribution.

VI. CONCLUSION

By introducing an operator-valued formalism for CTRWs, we have obtained the statistical properties of run-and-turn random motions, be they Poissonian or non-Poissonian. The model is versatile, describing all bacterial swimming patterns, Lévy walks, and with straightforward extensions to curved trajectories. We have provided throughout the text numerous analytical results. Except for the Lévy walks where only the asymptotic behavior was characterized, those explicit expressions are valid at all times. They should be helpful in rationalizing experimental data. In particular, the velocity correlation function may give insight into the type of swimming pattern, even without identifying turning events [113]. A recurrent finding is that memory in turning times may induce interesting features in motion properties. Using a gamma distribution of run time allows us to interpolate between the two extreme cases of no memory (Poissonian) and perfect memory (periodic). Through the interplay with rotational diffusion and turning angle, non-Poissonian patterns may lead to a minimum in velocity correlation function, and to a maximum of diffusivity at finite rotational diffusion or at finite curvature.

Though developed for swimming bacteria, the run-and-turn model considered here is applicable to a broad variety of situations. These include swimming organisms such as *Chlamydomonas Reinhardtii* and its eukaryotic version of the run-and-tumble pattern [114], self-propelled particles, whose random motions are receiving a renewed interest in the study of active matter [32,36,115–118], displacement of motor proteins on the network of cytoskeleton filaments [119,120], or animal foraging [27]. Run-and-turn motions are also relevant for individual cells [37,83,121], where a rich array of motility mechanisms is currently being explored, including crawling, gliding, or twitching [11]. In many contexts, it seems necessary to allow for a bimodal character. For example, the motor proteins exhibit frequent pauses during which they remain static on the filament [120], cells may migrate through a cycle of protrusion-retraction [37], the millimeter-sized zooplankton *Daphnia* moves through a series of ballistic hop and pause [122], and gulls may alternate between large-distance flights and pauses for rest or foraging [56]. Though very different in scale and nature, those instances of intermittent motion all suggest a run-stop pattern.

If the run-and-turn model provides a basic description, it does not exhaust all variations and there are many additional features that one would like to incorporate. Let us mention only

two examples. First, instead of being constant, the velocity may change in time, through a deterministic evolution [59], continuous fluctuations [123,124], or as a random variable chosen at the beginning of each run [38,125] as in the velocity jump model [25]. Second, rather than being independent quantities, run times may be correlated [126–128], a case that cannot be treated within the present formalism.

The natural world offers countless forms of random motions. It is tempting to think that many of them, having evolved for a given purpose or as tradeoff between competing requirements, are best adapted to a particular situation. Is this view warranted for the smallest form of life on the planet, bacteria? Much remains to be explored before one can fully assess the optimality of their swimming patterns. By providing the diffusion properties in a homogeneous environment, this work is a first step in this direction. Looking forward, the next step is to characterize how chemotaxis, the ability to navigate chemical gradients [41,129–131], depends on motion patterns.

APPENDIX A: TRANSFORMS AND CONVOLUTIONS

Here we summarize the definition and convolution property for the transforms introduced in the main text [132]. To avoid clutter of notation, the function and its transform are denoted with the same symbol, the nature of the function being indicated by the name of the variable. The time variable is treated with the Laplace transform

$$f(s) = \int_0^\infty dt\ e^{-st} f(t), \tag{A1a}$$

$$f(t) = \frac{1}{2\pi i} \int_{c-i\infty}^{c+i\infty} ds\ e^{ts} f(s), \tag{A1b}$$

$$[f * g](t) = \int_0^t dt'\ f(t-t')g(t'), \tag{A1c}$$

$$[f * g](s) = f(s)g(s). \tag{A1d}$$

For position $\mathbf{x}$ in dimension d, the Fourier transform is used:

$$f(\mathbf{k}) = \int_{\mathbb{R}^d} d\mathbf{r}\, e^{i\mathbf{k}\mathbf{r}} f(\mathbf{r}), \tag{A2a}$$

$$f(\mathbf{r}) = \frac{1}{(2\pi)^d} \int_{\mathbb{R}^d} d\mathbf{k}\, e^{-i\mathbf{k}\mathbf{r}} f(\mathbf{k}), \tag{A2b}$$

$$[f \star g](\mathbf{r}) = \int_{\mathbb{R}^d} d\mathbf{r}'\ f(\mathbf{r}-\mathbf{r}')g(\mathbf{r}'), \tag{A2c}$$

$$[f \star g](\mathbf{k}) = f(\mathbf{k})g(\mathbf{k}). \tag{A2d}$$

For orientation angle θ in $d = 2$, we employ the Fourier series

$$f(l) = \frac{1}{2\pi} \int_{-\pi}^{\pi} d\theta\, e^{-il\theta} f(\theta), \tag{A3a}$$

$$f(\theta) = \sum_{l=-\infty}^{\infty} f(l)\, e^{il\theta}, \tag{A3b}$$

$$[f \circ g](\theta) = \int_{-\pi}^{\pi} d\theta'\ f[pv(\theta-\theta')]g(\theta'), \tag{A3c}$$

$$[f \circ g](l) = 2\pi f(l)g(l), \tag{A3d}$$

where $pv(\theta) = \arg(e^{i\theta})$ with values taken in $]-\pi,\pi]$.

Finally, the spherical harmonic transform is needed for orientation in $d = 3$. Also called Laplace series or expansion, it is given by

$$f(l,m) = \int_0^{2\pi} d\phi \int_0^{\pi} \sin\theta\ d\theta \left[Y_l^m(\theta,\phi)\right]^* f(\theta,\phi), \tag{A4a}$$

$$f(\theta,\phi) = \sum_{l=0}^{\infty} \sum_{m=-l}^{l} f(l,m)\, Y_l^m(\theta,\phi). \tag{A4b}$$

Here $f(\theta,\phi)$ is a function defined on the unit sphere and having as arguments the polar and azimuthal angles θ and ϕ. The star denotes the complex conjugate. The spherical harmonic Y_l^m is

$$Y_l^m(\theta,\phi) = \sqrt{\frac{2l+1}{4\pi} \frac{(l-m)!}{(l+m)!}}\, P_l^m(\cos\theta) e^{im\phi}, \tag{A5}$$

where P_l^m is the associated Legendre function of degree l and order m. The Y_l^m are eigenfunctions for the angular part of the Laplacian in $d = 3$,

$$\Delta_a Y_l^m = -l(l+1)Y_l^m,$$
$$\Delta_a = \left[\frac{1}{\sin\theta}\partial_\theta\ \sin\theta\ \partial_\theta + \frac{1}{\sin^2\theta}\partial_{\phi\phi}^2\right]. \tag{A6}$$

For the turning events, we employ the azimuthally symmetric (or isotropic) convolution on the unit sphere, as used in geodesy and astrophysics applications [74,76],

$$[f \odot g](\theta,\phi) = \int_0^{2\pi} d\phi' \int_0^{\pi} \sin\theta'\, d\theta'\ f(\xi)\, g(\theta',\phi'), \tag{A7a}$$

$$[f \odot g](l,m) = \sqrt{\frac{4\pi}{2l+1}} f(l,0)\, g(l,m). \tag{A7b}$$

Here the function $f(\theta,\phi)$ is assumed to be azimuthally symmetric and accordingly denoted as $f(\theta)$. If $\mathbf{u} = (\sin\theta\cos\phi, \sin\theta\sin\phi, \cos\theta)$ is the unit vector with direction (θ,ϕ), $\xi = \arccos(\mathbf{u}\cdot\mathbf{u}')$ is the angle between (θ,ϕ) and (θ',ϕ'). Note that this convolution is not commutative. Only recently was a commutative anisotropic convolution defined on the unit sphere [75].

APPENDIX B: TECHNICAL STEPS

1. Operators in Laplace convolution

In Sec. II A, we used the operator representation and time Laplace transform to convert the integral $\int_0^t dt'\, g(t-t') \int d\mathbf{x}'\, p(\mathbf{x},\mathbf{x}',t-t') f(\mathbf{x}',t')$ into $g(s-\mathcal{L})f(\mathbf{x},s)$. This result, stated in Refs. [50] and [51], seems nonstandard. Here we provide some explanation for this step. Retracing the calculation backward, one can write

$$X = g(s-\mathcal{L})f(\mathbf{x},s), \tag{B1}$$
$$= \int_0^\infty dt''\, e^{-(s-\mathcal{L})t''} g(t'') \int_0^\infty dt'\, e^{-st'} f(\mathbf{x},t'),$$
$$= \int_0^\infty dt'' \int_0^\infty dt'\, g(t'') e^{-s(t''+t')} e^{t''\mathcal{L}} f(\mathbf{x},t'),$$

$$= \int_0^\infty dt \int_0^t dt'\, g(t-t') e^{-st} e^{(t-t')\mathcal{L}} f(\mathbf{x},t'),$$

$$X = \int_0^\infty dt\, e^{-st} \Bigg[\int_0^t dt'\, g(t-t') \times \int d\mathbf{x}'\, p(\mathbf{x},\mathbf{x}',t-t') f(\mathbf{x}',t') \Bigg].$$

The fourth line is obtained with the change of variable $t'' \to t = t'' + t'$, with $t \in [0,\infty)$ and $t' \in [0,t]$. In the last line, we applied the definition of operator representation as given by Eq. (4). The conclusion is that, paying attention to the ordering of terms, the usual convolution rule may be used with operator as argument.

2. Performing calculations

We describe here the main steps involved in the noncommutative calculations. Again, we consider only the model in $d = 2$, the case $d = 3$ being entirely analogous. For a function f, consider first the quantity

$$X = 2\pi \lim_{\substack{\mathbf{k}\to\mathbf{0} \\ l\to 0}} \left(-i \frac{\partial}{\partial k_x}\right) f(\hat{\mathcal{L}})\, P_{\rm in}(\mathbf{k},l). \tag{B2}$$

Such an expression arises for instance from the first term of Eq. (7), in which $f = \psi_\chi$. The initial probability density is $P_{\rm in}(\mathbf{r},\theta) = \delta(\mathbf{r})\delta(\theta)$, which translates into $P_{\rm in}(\mathbf{k},l) = 1/2\pi$. Since there is no differentiation with respect to k_y, the limit $k_y \to 0$ can be taken from the outset. Now, let us introduce $\epsilon = k_x$, $\mathrm{A} = s - D_{\rm r}\Delta_{\rm a}$ and $\mathrm{B} = -\frac{iv}{2}\mathrm{T}^+$, so that $\hat{\mathcal{L}} = \mathrm{A} + \epsilon\mathrm{B}$. Then, with the shorthand notation $\mathrm{A}(l) = s + D_{\rm r} l^2$,

$$X = -2\pi i \lim_{\substack{\epsilon\to 0 \\ l\to 0}} \frac{\partial}{\partial\epsilon} f(\mathrm{A}+\epsilon\mathrm{B}) \frac{1}{2\pi}, \tag{B3}$$

$$= -i \lim_{l\to 0} \overset{2}{\mathrm{B}}\, \delta f(\overset{1}{\mathrm{A}},\overset{3}{\mathrm{A}}),$$

$$= -\frac{v}{2} \lim_{l\to 0} \overset{2}{\mathrm{T}^+} \frac{f(\overset{1}{\mathrm{A}}) - f(\overset{3}{\mathrm{A}})}{\overset{1}{\mathrm{A}} - \overset{3}{\mathrm{A}}},$$

$$= -\frac{v}{2} \lim_{l\to 0} \sum_{j=-1,1} \frac{f(\mathrm{A}(l+j)) - f(\mathrm{A}(l))}{\mathrm{A}(l+j) - \mathrm{A}(l)},$$

$$X = v\, \frac{f(s) - f(s+D_{\rm r})}{D_{\rm r}}.$$

The second term in Eq. (7) is a product of operators, which can be expanded with the rule $(\mathrm{AB})' = \mathrm{A}'\mathrm{B} + \mathrm{AB}'$. To treat the $[1 - h(l)\psi(\mathrm{A}+\epsilon\mathrm{B})]^{-1}$ operator, however, the first and second derivatives are needed for a general term of the form $f(h(l)\psi(\mathrm{A}+\epsilon\mathrm{B}))$. Using the Daletskii-Krein formula leads to the following expression for the first order:

$$X_1 = \lim_{\epsilon\to 0} \frac{d}{d\epsilon} f(h(l)\psi(\mathrm{A}+\epsilon\mathrm{B})), \tag{B4}$$

$$X_1 = \overset{24}{h}\, \overset{22}{\mathrm{B}}\, \delta\psi(\overset{21}{\mathrm{A}},\overset{23}{\mathrm{A}})\, \delta f(\overset{10}{\mathrm{C}},\overset{30}{\mathrm{C}}),$$

TABLE I. Some instances of run-and-turn motions studied previously. Parameters not specified are arbitrary.

Motion	ψ	Parameters	Ref.
Unimodal	exponential		[40]
Bimodal		$D_{\rm r1} = D_{\rm r2}, \tau_1 = \tau_2$	[41]
Bimodal		$\alpha_1 = \alpha_2 = 0$	[39]
Bimodal		$v_1 = v_2, \alpha_1 = \alpha_2 = 1$	[133]
Run-stop	arbitrary	$v_2 = 0, \alpha_1 = 1,$	
		$D_{\rm r1} = D_{\rm r2} = 0$	[55]
Run-reverse		$\alpha = -1$	[70]
Run-reverse	$\delta(t-\tau)$	$\alpha = -1$	[134]

with the notation $\mathrm{C} = h\psi(\mathrm{A})$ and argument is implied for $h(l)$. As regards the second order, one finds

$$X_2 = \lim_{\epsilon\to 0} \frac{1}{2} \frac{d^2}{d\epsilon^2} f(h(l)\psi(\mathrm{A}+\epsilon\mathrm{B})), \tag{B5}$$

$$X_2 = \overset{26}{h}\, \overset{22}{\mathrm{B}}\, \overset{24}{\mathrm{B}}\, \delta^2\psi(\overset{21}{\mathrm{A}},\overset{23}{\mathrm{A}},\overset{25}{\mathrm{A}})\, \delta f(\overset{10}{\mathrm{C}},\overset{30}{\mathrm{C}}) + \overset{24}{h}\, \overset{22}{\mathrm{B}}\, \delta\psi(\overset{21}{\mathrm{A}},\overset{23}{\mathrm{A}})\, \overset{44}{h}\, \overset{42}{\mathrm{B}}\, \delta\psi(\overset{41}{\mathrm{A}},\overset{43}{\mathrm{A}})\, \delta^2 f(\overset{10}{\mathrm{C}},\overset{30}{\mathrm{C}},\overset{50}{\mathrm{C}}).$$

If made by hand, calculations are feasible at first order but become tedious for higher moments, which involve several differentiations. Accordingly, we resorted to a symbolic computation software, with a custom implementation of noncommutative rules.

APPENDIX C: CHECKS

1. Literature

A number of particular cases of run-and-turn motions have been previously investigated in the literature, as summarized in Table I. We have checked that those results for MSD, velocity correlation function, or diffusivity are recovered when applying our expressions. In the Poissonian class, Ref. [41] investigated a particular instance of bimodal motion, whereas Ref. [39] assumed isotropic turns, implying full randomization in orientation. In the non-Poissonian class, previous works considered a ballistic run-stop with isotropic turns [55], as well as unimodal run-reverse [70].

2. Simulations

For a further check, we have tested our results for the correlation function against direct numerical simulations, for the four cases detailed in Table II. Analytical formulas are provided in the text, except for the unimodal pattern with

TABLE II. Parameters used in simulations. In all cases, the run time is gamma distributed and the dimension is $d = 2$.

Case	Model	γ	Parameters	Eq.
A	unimodal	2	$D_{\rm r} = 0.1, \alpha = 2/\pi$	(C1)
B	unimodal	3	$D_{\rm r} = 0.1, \alpha = -1$	(33)
C	bimodal	2	$v_1 = v_2 = v, D_{\rm r1} = D_{\rm r2} = 0.2,$ $\tau_1 = \tau_2 = \tau, \alpha_1 = -1, \alpha_2 = 0$	(D4)
D	bimodal	2	$v_1 = 2v_2 = v, D_{\rm r1} = D_{\rm r2} = 0.3,$ $\tau_1 = \tau_2 = \tau, \alpha_1 = \alpha_2 = -1$	(40)

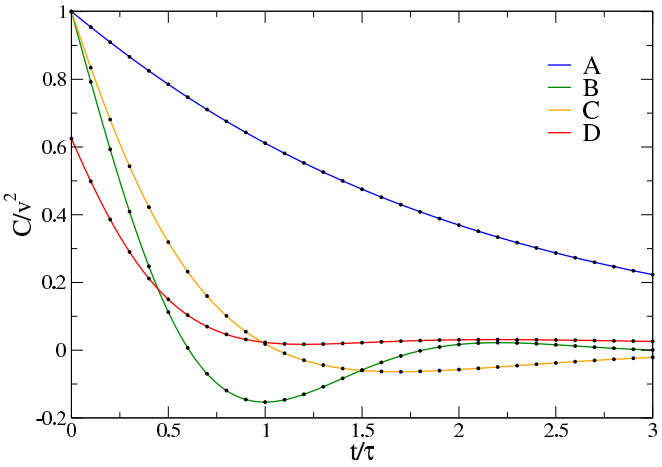

FIG. 13. Comparison between simulation (points) and analytical result (line) for the velocity correlation function in cases A to D described in Table II. The maximum absolute difference is less than 10^{-5}.

arbitrary α and $\gamma = 2$, for which

$$\frac{C(t)}{v^2} = \frac{e^{-(\tilde{D}_r+2/\tau)t}}{2}[(1+a)e^{t/\tau'} + (1-a)e^{-t/\tau'}], \quad \text{(C1)}$$

with $\tau' = \tau/(2\sqrt{\alpha})$ and $a = (1+\alpha)/(2\sqrt{\alpha})$. As visible in Fig. 13, the analytical and numerical results are in perfect agreement.

3. Moments in the Poissonian case

Here we explain how to compute moments of arbitrary order for the Poissonian unimodal motion. The run time distribution is $\psi(t) = \lambda e^{-\lambda t}$, with $\lambda = \tau^{-1}$ the rate of turning events. Let us consider the model in $d = 2$ and the equation governing its probability density $P(x,y,\theta,t)$,

$$\partial_t P = D_r \partial^2_{\theta\theta} P - v\cos\theta\,\partial_x P - v\sin\theta\,\partial_y P - \lambda P + \lambda\, h \circ P, \quad \text{(C2)}$$

where terms in the second line account for the turning events, and $\circ$ indicates convolution with respect to orientation variable θ as defined in Eq. (A3c). We introduce the moments with fixed orientation,

$$M_{nn'}(\theta,t) = \iint dx\; dy\; x^n y^{n'} P(x,y,\theta,t). \quad \text{(C3)}$$

Using Eq. (C2) and switching to transformed variables as in Sec. III A, one arrives at a recurrence formula in n,n' indices,

$$M_{nn'}(l,s) = (s + D_r l^2 + \lambda[1 - 2\pi h(l)])^{-1}\left[\delta_{n0}\delta_{n'0}\Theta_{in}(l) + \frac{v}{2}(n\mathrm{T}^+ M_{n-1,n'} + n'\mathrm{T}^- M_{n,n'-1})\right], \quad \text{(C4)}$$

where $\delta_{nn'}$ is the Kronecker delta, $\Theta_{in}(\theta)$ is the initial distribution of orientation, and $\mathrm{T}^\pm$ are operators as previously defined in Eq. (21). The moments are obtained by integrating over all possible orientations $M_{nn'}(s) = \int_{-\pi}^{\pi} d\theta\; M_{nn'}(\theta,s) = 2\pi M_{nn'}(l=0,s)$. In particular, the second moment in x is found to be

$$\langle x^2(s)\rangle = \frac{v^2}{s^2}\frac{2s\cos^2\theta_{in} + 4D_r + \bar{\kappa}}{(s + D_r + \kappa)(s + 4D_r + \bar{\kappa})}, \quad \text{(C5)}$$

where we have defined $\kappa = \lambda(1-\alpha)$, $\bar{\kappa} = \lambda(1-\bar{\alpha})$, $\bar{\alpha} = \langle\cos(2\theta)\rangle_h$ and have assumed a fixed orientation $\Theta_{in}(\theta) = \delta(\theta - \theta_{in})$.

An identical approach can be used in $d = 3$ and we only quote the end result. Assuming the initial orientation is azimuthally symmetric with fixed polar angle θ_{in}, the second moment in z is

$$\langle z^2(s)\rangle = \frac{2v^2}{3s^2}\frac{3s\cos^2\theta_{in} + 6D_r + \bar{\kappa}}{(s + 2D_r + \kappa)(s + 6D_r + \bar{\kappa})}. \quad \text{(C6)}$$

The general expression for arbitrary run time distribution is given by Eq. (D1) in $d = 2$ and Eq. (D2) in $d = 3$. When applied to the Poissonian case, they reduce to Eqs. (C5) and (C6), respectively. Because the latter were derived without recourse to noncommutative calculus, this provides one independent check of the procedure.

APPENDIX D: LONG FORMULAS

1. Unimodal run-and-turn

We report in this Appendix the second moment for unimodal motion with fixed initial orientation [135]. For $d = 2$, if the initial angle with respect to the x axis is fixed to θ_{in}, the second moment $\langle x^2\rangle$ is given by

$$\langle x^2(s)\rangle = \frac{M(s)}{2} + v^2 s\cos(2\theta_{in})\frac{C_1 + C_2\psi(s') + C_3\psi(s'') + C_4\psi(s')\psi(s'')}{3D_r\tau(ss's'')^2[1-\alpha\psi(s')][1-\bar{\alpha}\psi(s'')]}, \quad \text{(D1)}$$

$$C_1 = 3(4\alpha-5)D_r^2 + 3[(\alpha-2)s + \bar{\alpha}s' + \tau s's'']D_r,$$

$$C_2 = (16-13\alpha)D_r^2 + [(8-5\alpha)s + \bar{\alpha}(\alpha-4)s' - 3\alpha\tau s's'']D_r + (1-\alpha)s(s-\bar{\alpha}s'),$$

$$C_3 = 13\bar{\alpha}D_r^2 + \bar{\alpha}(5s - 3\tau s's'')D_r + \bar{\alpha}s^2 - (s')^2 - \alpha\bar{\alpha}(s'')^2 + \alpha s's'',$$

$$C_4 = 15\alpha\bar{\alpha}D_r^2 + 3(2\alpha\bar{\alpha}s - \alpha s' - \bar{\alpha}s'' + \alpha\bar{\alpha}\tau s's'')D_r,$$

with the notations $s' = s + D_r$, $s'' = s + 4D_r$, and $\bar{\alpha} = \langle\cos(2\theta)\rangle_h$. Moments of higher order in position would involve $s(l) = s + l^2 D_r$ and higher circular moments of the turning angle distribution $\alpha(l) = \langle\cos(l\theta)\rangle_h$ with $l \geqslant 3$.

For $d = 3$, we assume an initial orientation such that the polar angle (with respect to the z axis) is fixed to $\theta_{\rm in}$, and the azimuthal angle ϕ is uniformly distributed. Then the second moment $\langle z^2 \rangle$ is

$$\langle z^2(s) \rangle = \frac{M(s)}{3} + v^2 s \, \frac{3\cos^2(\theta_{\rm in}) - 1}{2} \, \frac{C_1 + C_2\psi(s') + C_3\psi(s'') + C_4\psi(s')\psi(s'')}{3D_{\rm r}\tau(ss's'')^2[1 - \alpha\psi(s')][1 - \bar{\alpha}\psi(s'')]}, \tag{D2}$$

$$C_1 = 8(3\alpha - 4){D_{\rm r}}^2 + 4[(\alpha - 2)s + \bar{\alpha}s' + \tau s's'']D_{\rm r},$$

$$C_2 = -48\alpha\tau {D_{\rm r}}^3 - 4(-9 + 7\alpha + 8\alpha\tau s){D_{\rm r}}^2 - 2[(4\alpha - 6)s + 2\alpha\tau s^2 + (3 - \alpha)\bar{\alpha}s']D_{\rm r} + (1 - \alpha)s(s - \bar{\alpha}s'),$$

$$C_3 = -48\bar{\alpha}\tau {D_{\rm r}}^3 - 4\bar{\alpha}(-7 + 9\alpha + 8\tau s){D_{\rm r}}^2 - 4\bar{\alpha}s(-2 + 3\alpha + \tau s)D_{\rm r} + \bar{\alpha}(1 - \alpha)s^2 - (s')^2 + \alpha s's'',$$

$$C_4 = 32\alpha\bar{\alpha}{D_{\rm r}}^2 + 4(2\alpha\bar{\alpha}s - \alpha s' - \bar{\alpha}s'' + \alpha\bar{\alpha}\tau s's'')D_{\rm r},$$

where $s' = s + 2D_{\rm r}$, $s'' = s + 6D_{\rm r}$, and $\bar{\alpha} = \langle (3\cos^2\theta - 1)/2 \rangle_h$. Higher moments in position would involve $s(l) = s + l(l + 1)D_{\rm r}$ and $\alpha(l) = \langle P_l(\cos\theta) \rangle_h$, where P_l is the Legendre polynomial of order l, with $l \geqslant 3$.

2. Bimodal run-and-turn

Finally, we give the velocity autocorrelation functions in terms of time variable for two particular bimodal motions that were used in Sec. IV B 1. Note that $d = 3$ in both cases. The first pattern involves no turning event ($\alpha_1 = \alpha_2 = 1$) and an exponential distribution of run time in both modes ($\gamma_1 = \gamma_2 = 1$). Other parameters are arbitrary. With the notation $D_{\rm r}^{\pm} = D_{\rm r1} \pm D_{\rm r2}$, the velocity correlation function is

$$C(t) = \frac{1}{2\tau'(\tau_1 + \tau_2)} \exp\left(\frac{-\tau'''t}{2\tau_1\tau_2}\right)\left\{v_1^2\tau_1((\tau' + \tau'')X + \tau' - \tau'') + S_{1\leftrightarrow 2} + 4v_1v_2\tau_1\tau_2(X - 1)\right\}, \tag{D3}$$

$$\tau' = \sqrt{(2\tau_1\tau_2 D_{\rm r}^-)^2 + 4\tau_1\tau_2(\tau_2 - \tau_1)D_{\rm r}^- + (\tau_1 + \tau_2)^2}, \quad \tau'' = \tau_1 - \tau_2 - 2D_{\rm r}^-\tau_1\tau_2,$$

$$\tau''' = \tau' + \tau_1 + \tau_2 + 2D_{\rm r}^+\tau_1\tau_2, \quad X = \exp\left(\frac{\tau' t}{\tau_1\tau_2}\right).$$

The second case is a run-reverse-flick motion with $\alpha_1 = -1$, $\alpha_2 = 0$, $v_1 = v_2 = v$, $D_{\rm r1} = D_{\rm r2} = D_{\rm r}$, and gamma distributed run time with $\gamma_1 = \gamma_2 = 2$. Then

$$C(t) = \frac{v^2\exp(-2D_{\rm r}t)}{(\tau_1 + \tau_2)(\tau_1 - \tau_2)^2}\left\{\exp(-2t/\tau_1)\left[\left(\tau_1^2 - 4\tau_1\tau_2 + 2\tau_2^2\right)t + \frac{\tau_1}{\tau_1 - \tau_2}\left(\tau_1^3 - 4\tau_1^2\tau_2 + 6\tau_1\tau_2^2 - 2\tau_2^3\right)\right] + S_{1\leftrightarrow 2}\right\}. \tag{D4}$$

[1] H. Berg, *E. coli in Motion* (Springer-Verlag, New York, 2004).
[2] K. Son, D. R. Brumley, and R. Stocker, Nat. Rev. Microbiol. **13**, 761 (2015).
[3] J. Elgeti, R. G. Winkler, and G. Gompper, Rep. Prog. Phys. **78**, 056601 (2015).
[4] E. Lauga, Annu. Rev. Fluid Mech. **48**, 105 (2016).
[5] H. Berg and D. Brown, Nature (London) **239**, 500 (1972).
[6] T. Pilizota, M. T. Brown, M. C. Leake, R. W. Branch, R. M. Berry, and J. P. Armitage, Proc. Natl. Acad. Sci. USA **106**, 11582 (2009).
[7] L. Xie, T. Altindal, S. Chattopadhyay, and X.-L. Wu, Proc. Natl. Acad. Sci. USA **108**, 2246 (2011).
[8] M. Theves, J. Taktikos, V. Zaburdaev, H. Stark, and C. Beta, Biophys. J. **105**, 1915 (2013).
[9] B. D. Hughes, *Random Walks and Random Environments* (Clarendon Press, Oxford, 1995).
[10] D. Bray, *Cell Movements: From Molecules to Motility* (Garland, New York, 2001).
[11] K. F. Jarrell and M. J. McBride, Nat. Rev. Microbiol. **6**, 466 (2008).
[12] R. Vogel and H. Stark, Phys. Rev. Lett. **110**, 158104 (2013).
[13] K. Son, F. Menolascina, and R. Stocker, Proc. Natl. Acad. Sci. USA **113**, 8624 (2016).
[14] G. Rosser, R. E. Baker, J. P. Armitage, and A. G. Fletcher, J. R. Soc. Interface **11**, 0320 (2014).
[15] J. E. Johansen, J. Pinhassi, N. Blackburn, U. L. Zweifel, and Å. Hagström, Aquat. Microb. Ecol. **28**, 229 (2002).
[16] K. Son, J. S. Guasto, and R. Stocker, Nat. Phys. **9**, 494 (2013).
[17] While in theoretical context run-and-tumble may describe any persistent motion interspersed with instantaneous reorientations, it can also refer to the particular turning mechanism of *E. coli*. The choice of a different appellation allows us to remove any ambiguity.
[18] L. G. Wilson, V. A. Martinez, J. Schwarz-Linek, J. Tailleur, G. Bryant, P. N. Pusey, and W. C. K. Poon, Phys. Rev. Lett. **106**, 018101 (2011).
[19] S. M. Vater, S. Weiße, S. Maleschlijski, C. Lotz, F. Koschitzki, T. Schwartz, U. Obst, and A. Rosenhahn, PLoS ONE **9**, e87765 (2014).
[20] K. M. Taute, S. Gude, S. J. Tans, and T. S. Shimizu, Nat. Commun. **6**, 8776 (2015).
[21] G. Rosser, A. G. Fletcher, D. A. Wilkinson, J. A. de Beyer, C. A. Yates, J. P. Armitage, P. K. Maini, and R. E. Baker, PLoS Comput. Biol. **9**, e1003276 (2013).
[22] P. P. Lele, T. Roland, A. Shrivastava, Y. Chen, and H. C. Berg, Nat. Phys. **12**, 175 (2015).

[23] Y. Tu and G. Grinstein, Phys. Rev. Lett. **94**, 208101 (2005).
[24] S. Chattopadhyay, R. Moldovan, C. Yeung, and X. L. Wu, Proc. Natl. Acad. Sci. USA **103**, 13712 (2006).
[25] H. Othmer, S. Dunbar, and W. Alt, J. Math. Biol. **26**, 263 (1988).
[26] E. Codling, M. Plank, and S. Benhamou, J. R. Soc. Interface **5**, 813 (2008).
[27] V. Mendéz, D. Campos, and F. Bartumeus, *Stochastic Foundations in Movement Ecology* (Springer-Verlag, Berlin, 2013).
[28] A. Stevens and H. G. Othmer, SIAM J. Appl. Math. **57**, 1044 (1997).
[29] D. Boyer and C. Solis-Salas, Phys. Rev. Lett. **112**, 240601 (2014).
[30] K. Pearson, Nature (London) **72**, 294 (1905).
[31] P. Kareiva and N. Shigesada, Oecologia **56**, 234 (1983).
[32] Z. Sadjadi, M. R. Shaebani, H. Rieger, and L. Santen, Phys. Rev. E **91**, 062715 (2015).
[33] J. Yuan and H. C. Berg, Proc. Natl. Acad. Sci. USA **111**, 15752 (2014).
[34] F. A. Haight, *Handbook of the Poisson Distribution* (John Wiley & Sons, New York, 1967).
[35] E. H. Hauge, Phys. Fluids **13**, 1201 (1970).
[36] D. Campos and V. Méndez, J. Chem. Phys. **130**, 134711 (2009).
[37] D. Campos, V. Méndez, and I. Llopis, J. Theor. Biol. **267**, 526 (2010).
[38] A. A. Pogorui and R. M. Rodríguez-Dagnino, J. Stat. Phys. **147**, 1216 (2012).
[39] F. Detcheverry, Eur. Phys. J. E **37**, 114 (2014).
[40] P. Lovely and F. Dahlquist, J. Theor. Biol. **50**, 477 (1975).
[41] J. Taktikos, H. Stark, and V. Zaburdaev, PLoS ONE **8**, e81936 (2013).
[42] E. A. Korobkova, T. Emonet, H. Park, and P. Cluzel, Phys. Rev. Lett. **96**, 058105 (2006).
[43] L. Xie, T. Altindal, and X.-L. Wu, PLoS ONE **10**, e0141654 (2015).
[44] M. Theves, J. Taktikos, V. Zaburdaev, H. Stark, and C. Beta, Europhys. Lett. **109**, 28007 (2015).
[45] M. Morse, J. Bell, G. Li, and J. X. Tang, Phys. Rev. Lett. **115**, 198103 (2015).
[46] Y. Tu, Proc. Natl. Acad. Sci. USA **105**, 11737 (2008).
[47] S. B. van Albada, S. Tnase-Nicola, and P. R. ten Wolde, Mol. Syst. Biol. **5**, 316 (2009).
[48] E. Korobkova, T. Emonet, J. Vilar, T. Shimizu, and P. Cluzel, Nature (London) **428**, 574 (2004).
[49] F. Matthäus, M. S. Mommer, T. Curk, and J. Dobnikar, PLoS ONE **6**, e18623 (2011).
[50] S. Eule, R. Friedrich, F. Jenko, and I. M. Sokolov, Phys. Rev. E **78**, 060102 (2008).
[51] H. Affan, R. Friedrich, and S. Eule, Phys. Rev. E **80**, 011137 (2009).
[52] E. Montroll and G. Weiss, J. Math. Phys. **6**, 167 (1965).
[53] J. Klafter and I. M. Sokolov, *First Steps in Random Walks* (Oxford University Press, Oxford, 2011).
[54] F. Thiel, L. Schimansky-Geier, and I. M. Sokolov, Phys. Rev. E **86**, 021117 (2012).
[55] L. Angelani, Europhys. Lett. **102**, 20004 (2013).
[56] J. P. Taylor-King, E. E. van Loon, G. Rosser, and S. J. Chapman, Bull. Math. Biol. **77**, 1213 (2015).
[57] F. Detcheverry, Europhys. Lett. **111**, 60002 (2015).
[58] J. Haus and K. Kehr, Phys. Rep. **150**, 263 (1987).
[59] J. Liu, B. Yang, X. Chen, and J.-D. Bao, Eur. Phys. J. B **88**, 88 (2015).
[60] J. Masoliver, M. Montero, J. Perelló, and G. H. Weiss, Physica A **379**, 151 (2007).
[61] "Liouvillian" is used here as a convenient term for the linear operator involved in the Fokker-Planck equation describing the run. Dynamics which do not conserve probability, such as the chemical reactions considered in Ref. [50], might be handled as well, but will not be considered in this work.
[62] J. Tunaley, J. Stat. Phys. **14**, 461 (1976).
[63] G. Zumofen and J. Klafter, Phys. Rev. E **47**, 851 (1993).
[64] W. Feller, *An Introduction to Probability Theory and its Applications* (John Wiley & Sons, New York, 1968).
[65] S. Eule and R. Friedrich, Phys. Rev. E **87**, 032162 (2013).
[66] R. P. Feynman, Phys. Rev. **84**, 108 (1951).
[67] R. Metzler, J.-H. Jeon, A. G. Cherstvy, and E. Barkai, Phys. Chem. Chem. Phys. **16**, 24128 (2014).
[68] V. Nazaikinskii, V. Shatalov, and B. Sternin, *Methods of Noncommutative Analysis* (de Gruyter, Berlin, 1996).
[69] This assumption is motivated by applications to bacteria. The formalism can handle asymmetric distributions of turning angle.
[70] R. Großmann, F. Peruani, and M. Bär, New J. Phys. **18**, 043009 (2016).
[71] V. Zaburdaev, I. Fouxon, S. Denisov, and E. Barkai, Phys. Rev. Lett. **117**, 270601 (2016).
[72] Upon converting convolution in $\mathbf{x}$ to product in $\mathbf{q}$, a numerical constant C may appear. For simplicity, Eq. (7) assumes $C = 1$. Extension to $C \neq 1$ is straightforward.
[73] In particular, we use the relation $\cos\theta\, Y_l^m = a_{l+1}^m Y_{l+1}^m + a_l^m Y_{l-1}^m$, with $a_l^m = [\frac{(l-m)(l+m)}{(2l-1)(2l+1)}]^{1/2}$ [132].
[74] R. A. Kennedy, T. A. Lamahewa, and L. Wei, Digit. Signal Process. **21**, 660 (2011).
[75] P. Sadeghi, R. A. Kennedy, and Z. Khalid, IEEE T. Signal. Process. **60**, 6697 (2012).
[76] M. Tegmark, D. Hartmann, M. Briggs, and C. Meegan, Astrophys. J. **468**, 214 (1995).
[77] Because like the Laplace variable s, $\tilde{D}_r = (d-1)D_r$ is the reciprocal of a time, the notation $\psi(\tilde{D}_r)$ implicitly assumes $\psi(s = \tilde{D}_r)$.
[78] A similar observation holds for discrete random walks where the MSD or $\mathcal{D}$ depend only on α [31,32].
[79] This can be deduced from Eq. (31) for $\psi(s)$, as in the intracellular clock model proposed in Ref. [70]
[80] R. Gorenflo, A. A. Kilbas, F. Mainardi, and S. V. Rogosin, *Mittag-Leffler Functions, Related Topics and Applications* (Springer, Heidelberg, 2014).
[81] Those expressions, obtained in Ref. [57], were also derived in Ref. [70] by a different method.
[82] In the case $\gamma = 2$ for instance, extrema occur at $3\pi/8 + n\pi/2$, with n a positive integer. Note also that in the limit of periodic turning, motion would be reciprocal and $C(t)$ a square wave.
[83] L. Golé, C. Rivière, Y. Hayakawa, and J.-P. Rieu, PLoS ONE **6**, e26901 (2011).
[84] This conclusion does not apply to Poissonian models that are bimodal [41].
[85] In the particular case $\alpha = -1$, Eq. (4.8) of Ref. [70] is recovered.

[86] Using Eq. (35), the exact expression is $\gamma_c = (\alpha - 1)(3 + 3\alpha + \sqrt{1 - 14\alpha + \alpha^2})/[2(1 + 4\alpha + \alpha^2)]$.

[87] J. Saragosti, P. Silberzan, and A. Buguin, PLoS ONE **7**, e35412 (2012).

[88] The final result is independent of the choice of convention, as it should be.

[89] See Table I in Ref. [21]

[90] One has $\alpha = \int_0^\infty dt\, \psi_2(t)\langle\cos\theta(t)\rangle$, where $\langle\cos\theta(t)\rangle = \exp(-2D_{r2}t)$ for rotational diffusion, leading to $\alpha = \psi_2(s = 2D_{r2})$, with $\psi_2(s) = 1/(1 + \tau_2 s)$ for an exponentially distributed run time. Note that for *E. coli*, taking $\alpha = 0.33$ [136] and $\tau_2 = 0.14$ s [5] leads to $D_{r2} \simeq 7$ rad^2 s^{-1}, an estimate twice higher than that of Ref. [87].

[91] We took $D_{r1} \simeq 0.2$ rad^2 s^{-1} [41], and D_{r2} at least ten times higher, as suggested by the result $D_{r2} = 3.5$ rad^2 s^{-1} found in Ref. [87].

[92] Note that in the limit of vanishing D_r, $C(t)$ approaches a constant at long time, implying a divergence of diffusivity. This is expected as the trajectory becomes unidirectional with on average a net displacement at each cycle, thus leading to ballistic motion.

[93] M. Morse, R. Colin, L. G. Wilson, and J. X. Tang, Biophys. J. **110**, 2076 (2016).

[94] E. Lauga, W. R. DiLuzio, G. M. Whitesides, and H. A. Stone, Biophys. J. **90**, 400 (2006).

[95] A. P. Berke, L. Turner, H. C. Berg, and E. Lauga, Phys. Rev. Lett. **101**, 038102 (2008).

[96] M. Molaei, M. Barry, R. Stocker, and J. Sheng, Phys. Rev. Lett. **113**, 068103 (2014).

[97] K. Erglis, Q. Wen, V. Ose, A. Zeltins, A. Sharipo, P. A. Janmey, and A. Cēbers, Biophys. J. **93**, 1402 (2007).

[98] S. Ebbens, R. A. L. Jones, A. J. Ryan, R. Golestanian, and J. R. Howse, Phys. Rev. E **82**, 015304 (2010).

[99] F. Kümmel, B. ten Hagen, R. Wittkowski, I. Buttinoni, R. Eichhorn, G. Volpe, H. Löwen, and C. Bechinger, Phys. Rev. Lett. **110**, 198302 (2013).

[100] B. Gutiérrez-Medina, A. J. Guerra, A. I. P. Maldonado, Y. C. Rubio, and J. V. G. Meza, Phys. Biol. **11**, 066006 (2014).

[101] S. van Teeffelen and H. Löwen, Phys. Rev. E **78**, 020101 (2008).

[102] C. Weber, P. K. Radtke, L. Schimansky-Geier, and P. Hänggi, Phys. Rev. E **84**, 011132 (2011).

[103] For periodic turning ($\gamma = \infty$), $\mathcal{D}(\Omega)$ vanishes, except at discrete values where it is infinite. At $\tau\Omega = (2n + 1)\pi$, the turning event exactly cancels the angular drift occurring during a run and motion is ballistic.

[104] Indeed, using respectively τ and $v\tau$ as time and distance units, the small-Ω expansion is $\mathcal{D}(\Omega) = 1/(4\gamma) + (\gamma^2 - 2)/(16\gamma^3)\Omega^2 + O(\Omega^4)$.

[105] L. Haeggqwist, L. Schimansky-Geier, I. M. Sokolov, and F. Moss, Eur. Phys. J. Spec. Top. **157**, 33 (2008).

[106] C. Weber, I. M. Sokolov, and L. Schimansky-Geier, Phys. Rev. E **85**, 052101 (2012).

[107] G. Ariel, A. Rabani, S. Benisty, J. D. Partridge, R. M. Harshey, and A. Be'er, Nat. Commun. **6**, 8396 (2015).

[108] V. Zaburdaev, S. Denisov, and J. Klafter, Rev. Mod. Phys. **87**, 483 (2015).

[109] This is in agreement with Eq. (13) of Ref. [40].

[110] The velocity has to be rescaled for the product model.

[111] A. Godec and R. Metzler, Phys. Rev. Lett. **110**, 020603 (2013).

[112] D. Froemberg and E. Barkai, Phys. Rev. E **87**, 030104 (2013).

[113] The velocity correlation function can be obtained from raw data by twice differentiating the MSD. In practice, the latter may first be fitted to any adequate function so that differentiation does not induce excessive numerical noise.

[114] M. Polin, I. Tuval, K. Drescher, J. P. Gollub, and R. E. Goldstein, Science **325**, 487 (2009).

[115] F. J. Sevilla and L. A. Gómez Nava, Phys. Rev. E **90**, 022130 (2014).

[116] J. Nötel, I. M. Sokolov, and L. Schimansky-Geier, J. Phys. A **50**, 034003 (2017).

[117] M. E. Cates, Rep. Prog. Phys. **75**, 042601 (2012).

[118] M. C. Marchetti, J. F. Joanny, S. Ramaswamy, T. B. Liverpool, J. Prost, M. Rao, and R. A. Simha, Rev. Mod. Phys. **85**, 1143 (2013).

[119] M. R. Shaebani, Z. Sadjadi, I. M. Sokolov, H. Rieger, and L. Santen, Phys. Rev. E **90**, 030701 (2014).

[120] A. E. Hafner, L. Santen, H. Rieger, and M. R. Shaebani, Sci. Rep. **6**, 37162 (2016).

[121] D. Selmeczi, L. Li, L. I. Pedersen, S. F. Nrrelykke, P. H. Hagedorn, S. Mosler, N. B. Larsen, E. C. Cox, and H. Flyvbjerg, Eur. Phys. J. Spec. Top. **157**, 1 (2008).

[122] R. Garcia, F. Moss, A. Nihongi, J. R. Strickler, S. Göller, U. Erdmann, L. Schimansky-Geier, and I. M. Sokolov, Math. Biosci. **207**, 165 (2007).

[123] C. A. Condat, J. Jäckle, and S. A. Menchón, Phys. Rev. E **72**, 021909 (2005).

[124] P. Romanczuk and L. Schimansky-Geier, Phys. Rev. Lett. **106**, 230601 (2011).

[125] A. De Gregorio, Adv. Appl. Probab. **42**, 1028 (2010).

[126] J. H. P. Schulz, A. V. Chechkin, and R. Metzler, J. Phys. A **46**, 475001 (2013).

[127] A. V. Chechkin, M. Hofmann, and I. M. Sokolov, Phys. Rev. E **80**, 031112 (2009).

[128] V. Tejedor and R. Metzler, J. Phys. A **43**, 082002 (2010).

[129] M. J. Schnitzer, Phys. Rev. E **48**, 2553 (1993).

[130] J. T. Locsei, J. Math. Biol. **55**, 41 (2007).

[131] L. Xie and X.-L. Wu, Biophys. J. **107**, 1712 (2014).

[132] G. Arfken, H. Weber, and F. Harris, *Mathematical Methods for Physicists* (Academic Press, Oxford, 2013).

[133] J. d'Alessandro, A. P. Solon, Y. Hayakawa, C. Anjard, F. Detcheverry, J.-P. Rieu, and C. Rivière, Nat. Phys. (2017).

[134] E. Lauga, Phys. Rev. Lett. **106**, 178101 (2011).

[135] The first moment directly derives from the MSD, with $\langle x(s)\rangle$ and $\langle z(s)\rangle$ equal to $\cos(\theta_{in})sM(s)/(2v)$ for $d = 2$ and 3 respectively.

[136] H. C. Berg, *Random Walks in Biology* (Princeton University Press, Princeton, NJ, 1983).